computation

MDPI

Article

Power Quality Analysis of a Microgrid-Based on Renewable Energy Sources: A Simulation-Based Approach

Emmanuel Hernández-Mayoral [1,*], Christian R. Jiménez-Román [2], Jesús A. Enriquez-Santiago [3], Andrés López-López [4], Roberto A. González-Domínguez [5], Javier A. Ramírez-Torres [4], Juan D. Rodríguez-Romero [2] and O. A. Jaramillo [2]

1 CONAHCYT Attached at Instituto de Energías Renovables, Universidad Nacional Autónoma de México, Priv. Xochicalco s/n, Temixcio 62580, Mexico
2 Instituto de Energías Renovables, Universidad Nacional Autónoma de México, Priv. Xochicalco s/n, Temixcio 62580, Mexico; crjiro@ier.unam.mx (C.R.J.-R.); jdrr@ier.unam.mx (J.D.R.-R.); ojs@ier.unam.mx (O.A.J.)
3 Division of Graduate Studies, Isthmus University, Tehuantepec 70760, Mexico; ing.jesusantonio@hotmail.com
4 Centro de Investigación, Innovación y Desarrollo Tecnológico (CIIDETEC-UVM), Universidad del Valle de México, Tuxtla Gutiérrez 29056, Mexico; andres.lopez@uvmnet.edu (A.L.-L.); javier.ramirezt@e.unicach.mx (J.A.R.-T.)
5 Instituto de Investigación e Innovación en Energías Renovables, Universidad de Ciencias y Artes de Chiapas, Tuxtla Gutiérrez 29014, Mexico; roberto.gonzalezd@uvmnet.edu
* Correspondence: emhema@ier.unam.mx

Abstract: At present, microgrids (μGs) are a focal point in both academia and industry due to their capability to sustain operations that are stable, resilient, reliable, and of high power quality. Power converters (PCs), a vital component in μGs, enable the decentralization of power generation. However, this decentralization introduces challenges related to power quality. This paper introduces a μG model, based on the IEEE 14-bus distribution system, with the objective of investigating power quality when the μG is operating in conjunction with the conventional power grid. The μG model was developed using MATLAB-Simulink®, a tool specialized for electrical engineering simulations. The results obtained undergo thorough analysis and are compared with the compatibility levels set by the IEEE-519 standard. This method enables a precise evaluation of the μGs' capacity to maintain acceptable power quality levels while interconnected with the conventional power grid. In conclusion, this study contributes significantly to the field of μGs by providing a detailed and quantitative assessment of power quality. This will assist in the design and optimization of μGs for effective implementation in real-world electric power systems.

Keywords: microgrids; power quality; total harmonic distortion

Citation: Hernández-Mayoral, E.; Jiménez-Román, C.R.; Enriquez-Santiago, J.A.; López-López, A.; González-Domínguez, R.A.; Ramírez-Torres, J.A.; Rodríguez-Romero, J.D.; Jaramillo, O.A. Power Quality Analysis of a Microgrid-Based on Renewable Energy Sources: A Simulation-Based Approach. *Computation* **2024**, *12*, 226. https://doi.org/10.3390/computation12110226

Received: 2 August 2024
Revised: 4 October 2024
Accepted: 4 November 2024
Published: 12 November 2024

1. Introduction

As the demand for electric energy intensifies, the role of Distributed Generation Units (DGUs) in improving power quality becomes increasingly vital. DGUs offer numerous advantages such as reduced energy losses, decreased greenhouse gas emissions, enhanced voltage regulation, and superior supply reliability compared to traditional centralized generations. These benefits make DGUs an essential component of the electric microgrid (μG) [1].

The μG, a system that includes loads, DGUs, and Energy Storage Systems (ESSs), operates autonomously and independently from the conventional distribution system. This independence ensures the continuity and reliability of the electric supply [2–5].

However, the extensive integration of DGUs, such as photovoltaic (PV) systems and wind power generation, along with power electronics-based devices, can result in load unbalances and non-linearity in μGs. These factors can significantly affect the power quality

of the entire μG, leading to voltage issues like distortion, fluctuations, and variations. These issues have the potential to destabilize the μG system [6,7].

Microgrids, or μGs, have the capability to operate in two distinct modes: the islanding mode and the grid-connected mode. The islanding mode is more vulnerable to disturbances such as distortion or voltage unbalance, primarily due to the high system impedance. Conversely, the grid-connected mode is susceptible to issues like harmonic distortion and grid unbalances [8].

These problems can lead to complications including poor performance of protection relays, overheating of motors and transformers, and capacitor failure, which can subsequently impact the power factor (PF) [9,10]. Therefore, it is of utmost importance to maintain high power quality for all users, whether they are basic or commercial [11].

1.1. State of the Art

Despite the rising significance of microgrids (μGs), there is a noticeable gap in research focusing on power quality within these systems [12]. The majority of studies tend to focus on larger electrical grids, leaving a void in the understanding of μGs. However, a few existing studies, such as [13], have begun to bridge this gap.

In the study in [13], the authors utilized DSS® software to analyze the power quality of a hybrid μG, consisting of a PV system, battery-based Energy Storage Systems (BESSs), and capacitive loads. They discovered that the Total Harmonic Distortion (THD) values of voltage and current increased with the penetration of the PV system in the μG. In another study [14], the authors evaluated the power quality of a μG incorporating DGUs and operating in both modes. The μG was simulated using MATLAB-Simulink software across four different scenarios. The findings indicated that the integration of the μG significantly influenced the current and voltage THD ratios when the μG operated in islanding mode. The implementation of a harmonic filter was suggested to mitigate the magnitude of the harmonic content present in the μG.

In the study in [15], the authors developed an experimental assessment of harmonic distortion occurring at the Point of Common Coupling (PCC) of several PV inverters connected to the power grid. The study included the assessment of long-term power quality parameters according to EN 50160 [16], such as nominal frequency deviations, RMS voltage variations, voltage fluctuations (flickers), voltage imbalance and THD. The case study analyzed two different working conditions of the distribution system: before and after implementing the μG. The study concluded that the current harmonics generated by the PV system are highly dependent on the generation level; i.e., at a high generation level, harmonic distortion is relatively low (<5%). The authors in [17] analyzed the power quality in a μG considering both different levels of renewable energy penetration (33.3%, 66.6%, and 99.9%) and different meteorological conditions. They concluded that as the renewable penetration increases, power quality problems worsen in μGs.

In a study by the authors of [18], PSS-SINCAL was used to model an AC-μG with a PV system. The study analyzed the power quality problems of the system and found that solar disturbances caused voltage fluctuations at the local bus and high voltage THD at the non-linear load bus. In another study by the authors of [19], three power quality problems, namely voltage unbalances, waveform distortion, and voltage THD, were analyzed. It was observed that non-linear loads were more affected by solar energy penetration than linear loads, and the voltage THD exceeded the IEEE-519 standard [20] limit of 5%. In a study reported in [21], an AC-μG was evaluated experimentally, and it was verified that its voltage THD was within the IEEE-519 limit. However, the current THD increased as solar generation decreased due to shading or cloud effects. The study concluded that the current THD stayed below the IEEE-519 limit of 5% when solar generation was above 60%.

In more recent studies, the authors of [22] developed an investigation about the harmonic distortion capacity of a PV system in an AC-μG. The research work details the modeling of the μG composed of two PV systems, a battery-based ESS and programmable loads. The μG is connected to the electrical grid. MATLAB/Simulink® software is used to

model the AC-μG. The results of the study declare that power quality improves with the use of harmonic compensation techniques for μG applications affected by disturbances in the electrical grid. In [23], the authors analyze variables such as active power, reactive power, PF, THD and frequency in the static loads of an electrical μG composed of a PV–wind system and in static loads of appliances using a high-speed power meter with accuracy, low cost and high performance, alongside IoT functionality, to collect power quality data. The research results help optimize energy distribution and ensure proper functioning of the electrical μG infrastructure. The authors in [24] design and analyze some power quality aspects in an electrical μG made up of a three-phase PV system and composite non-linear loads located at different interconnection points of the μG. The authors used cross-frequency admittance matrix theory to model the loads. The complete μG model was simulated in the MATLAB/Simulink® environment. The purpose of this study is to analyze the impact on the power quality of a PV system connected to the electrical μG when there are compound non-linear loads. The power quality aspects evaluated are power distortion, waveform distortion and system imbalance.

1.2. Paper Motivation, Contribution, and Organization

In summary, the majority of research studies in the literature display specific characteristics determined by the configuration, topology, and the particular components utilized in the μGs under study. Each study tackles various challenges such as the dynamics and limited capacity of ESSs, the diversity of DGUs, power converters (PCs), and the significant presence of non-linear loads. Some methodologies opt to model each DGU, simplifying the model to a linear and time-invariant system, characterized by a constant and a gain factor, without considering the dynamics of the grid. Therefore, each study carried out in the literature addresses a specific challenge with characteristics very specific to each μG.

To bridge this gap, our paper scrutinizes key aspects of power quality in a 14-bus hybrid μG based on the original IEEE 14-bus distribution system, which is a representation of a simple approximation of the US electrical power system. This grid topology has been selected because it has the same structure as a conventional grid, provided that the lengths of the distribution lines, the capacities of the generators, the types of loads, etc., are readjusted, and above all, it maintains the same production of electrical energy. We consider the characteristics of DGUs in a steady state, voltage fluctuations, the nature of the load, the dynamics of ESSs, and a maximum demand scenario. Our findings are benchmarked against the IEEE-519 standard. The most significant contributions include the following:

- A fully detailed 14-bus μG system operating in grid-connected mode for power quality studies has been designed and modeled. Within this μG, various DGUs, including solar and wind power sources, as well as both balanced and unbalanced loads (comprising linear and non-linear loads), BESSs, power transformers, and distribution lines, have been considered. It is worth mentioning that the proposed μG model is a variation of the original IEEE 14-bus model and that no previous study has analyzed the impact of wind generation on μGs. The details of this impact are discussed in Section 5.
- Certain PCs have been considered, implementing both open-loop and closed-loop control strategies. Notably, these rectifiers or inverters utilize pulse width modulation (PWM) techniques with varying carrier frequencies. However, no advanced control schemes or any proposals for mitigation of power quality problems have been proposed. These topics are outside the scope of this research. However, the technical aspects of the inverters/rectifiers of the DGUs that make up the electrical μG are clearly described, unlike previous studies that omit this information.
- This study focuses on a proposed μG with a capacity of 4 MW, where 75% of the power is received from conventional generation based on a 3 MW diesel generator. The study examines various parameters, including voltage and PF variations in each bus of the μG, and voltage and current THD index variations. The relevance of the study is analyzed by comparing it with the IEEE-519 standard and with other studies that address these same problems. Furthermore, the conflicts caused by the bidirectional

flow of energy and the inclusion of DGUs such as PV systems and especially wind systems are detailed, knowing that the latter, being a non-dispatchable plant, tends to inject a greater harmonic content into the electric μG.

- Finally, a comparative study of different studies carried out in the last three years related to power quality issues for applications in electrical μGs is presented. This review has been carried out as a validation tool of the results obtained in this research with respect to the results of other studies, highlighting the DGUs implemented, the types of loads selected and the impact of incorporating an electrical DC-μG into the system.

In conclusion, this work serves as a foundation for examining current topics in μGs, including optimization techniques, fault diagnosis, system identification, and fault-tolerant control. These subjects will be delved into more deeply in future research. The structure of the document is as follows: Section 2 addresses the general aspects of μGs, including their composition, structure, operation modes, classification, and current challenges. Section 3 provides a detailed description of the design and modeling of the proposed hybrid μG for power quality studies. The hybrid μG model is implemented using MATLAB-Simulink® software. Section 4 presents the results obtained from the hybrid μG operating in the electrical grid-connected mode and compares them with the IEEE-519 standard. Section 5 critically analyzes the results obtained in this research and compares them with other similar studies. Finally, Section 6 summarizes the most important conclusions of this research.

2. Microgrid Generalities

μGs are small-scale electrical power systems (EPSs) composed of DGUs, ESSs, PCs, AC-DC buses, mixed loads, control units, a monitoring system and software interfaces. Compared to conventional EPSs, the modeling and simulation of μGs are more complex. Consequently, the implementation of models that facilitate dynamic analysis becomes a crucial element to guarantee the operational stability of future μGs.

2.1. Microgrid Architecture

μGs are compact EPSs that consist of DGUs, ESSs, PCs, AC-DC buses, a variety of loads, control units, monitoring systems, and software interfaces, as seen in Figure 1. When compared to traditional EPSs, the modeling and simulation of μGs present a higher level of complexity. As a result, the development of models that enable dynamic analysis is essential to ensure the operational stability of future μGs.

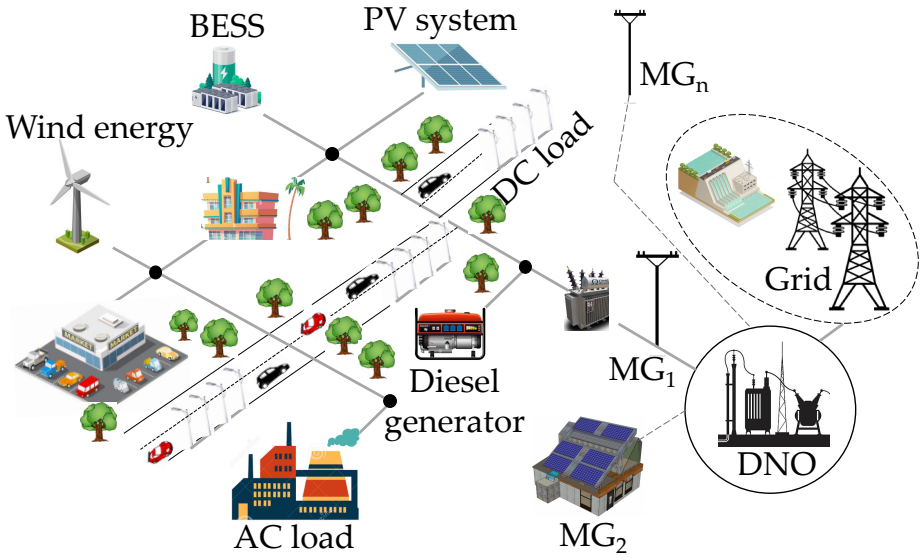

Figure 1. Typical diagram of a μG [3].

2.1.1. AC Microgrid (AC-μG)

The schematic of an AC microgrid (AC-μG) is depicted in Figure 2. In this diagram, all DGUs, including ESSs and loads, are connected to AC buses through a PC. It is worth noting that AC generators, such as hydro-turbines, diesel, and wind generators, can be directly connected to the power grid without the need for a PC. However, to incorporate DGUs like PV systems and BESSs into the power grid, a DC-AC PC is necessary [25].

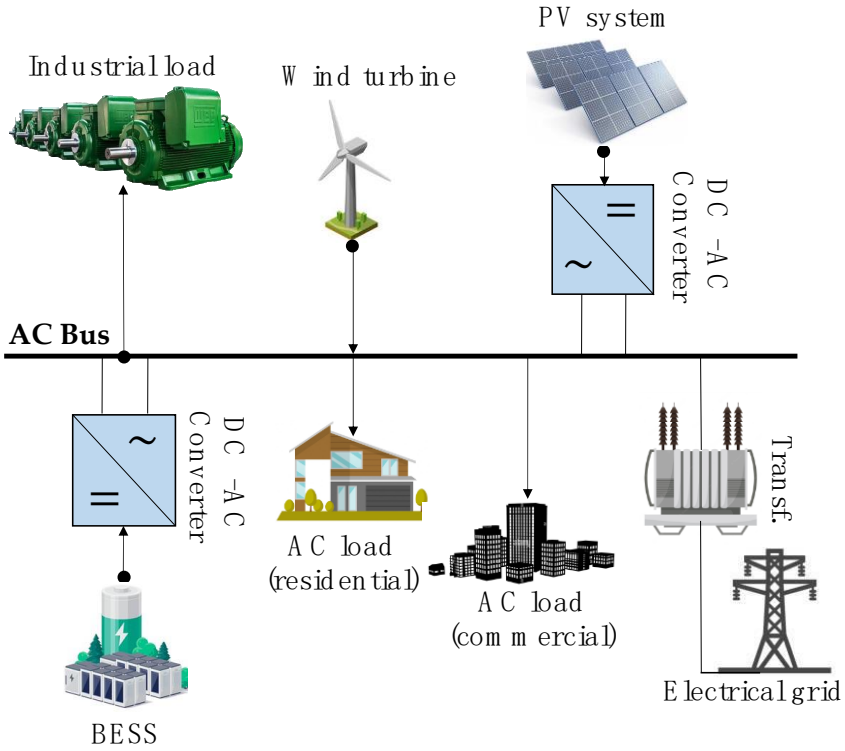

Figure 2. Typical diagram of an AC-μG [25].

2.1.2. DC Microgrid (DC-μG)

Most generators within a μG produce DC electricity. This DC output must be converted into AC to align with the grid system. At the system's end, a conversion back to DC is necessary because certain devices require AC power for their operation. However, this DC/AC/DC transformation in an AC-μG can decrease efficiency and lead to energy loss. This problem can be mitigated by using High-Voltage Direct Current (HVDC) operation as a reference. The DC-μG has been specifically engineered to address this issue [26]. The configuration of a DC-μG, as depicted in Figure 3, is distinct from an AC-μG.

2.1.3. AC-DC or Hybrid Microgrid

A hybrid μG involves connecting AC and DC grids using bidirectional PCs. This setup reduces the number of conversion steps required in individual DC or AC μGs, which helps prevent power quality issues. In a hybrid μG, DC-DGUs and loads are linked to the DC grid, while AC-DGUs and loads are connected to the AC grid. The diagram in Figure 4 shows the typical configuration of a hybrid μG, highlighting the reduction in conversion stages by eliminating the inversion stage in the PV system and BESS. The distinction between AC and DC loads is clear, as both grids are connected through a single bidirectional coupling point. These μGs can operate in grid-connected mode to either supply power to or consume power from a conventional grid, catering to the demands of power generation and loads. In grid-connected operation, the μG operates efficiently to ensure a reliable power supply to the critical load. However, in the event of disturbances, the μG must disconnect from the power grid and switch to islanding mode. The transition during this mode change must be

properly controlled to prevent damage to the μG devices. Therefore, power quality issues require further research in this context [27].

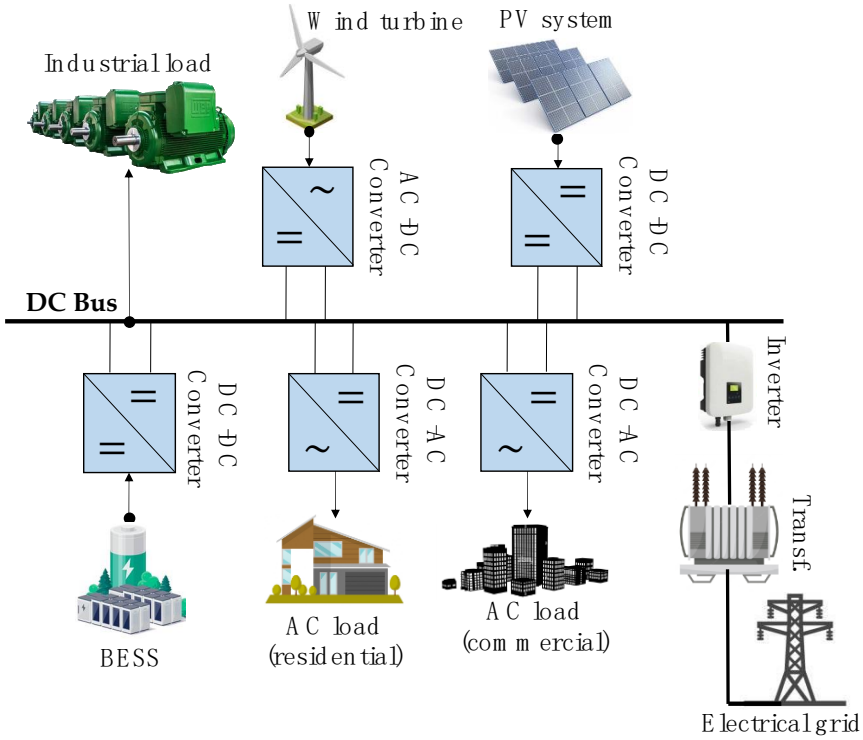

Figure 3. Typical diagram of a DC-μG [26].

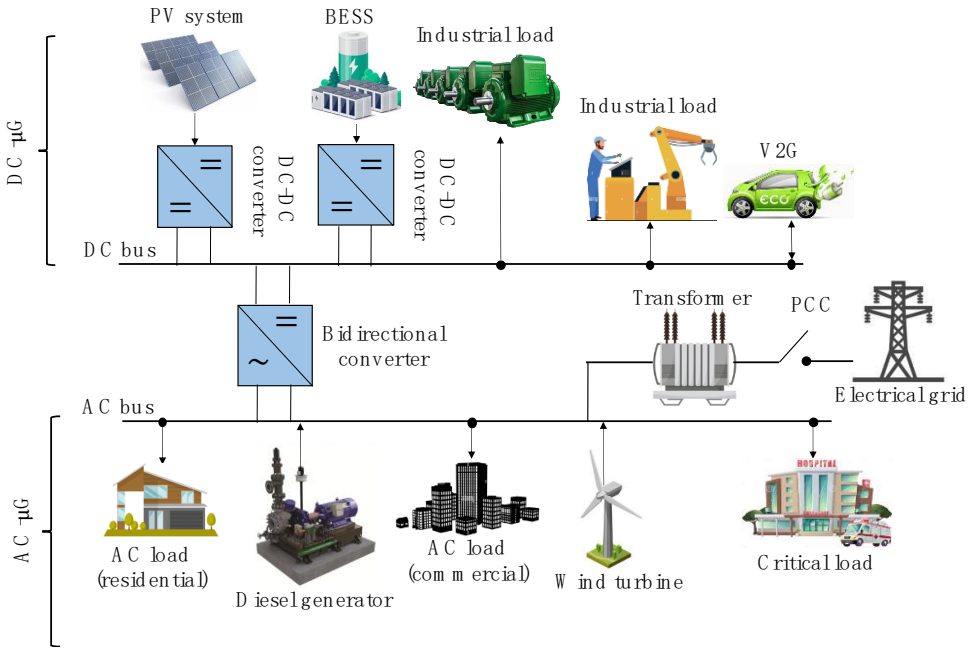

Figure 4. Typical diagram of a DC-AC or hybrid microgrid [27].

2.2. Microgrid Operation Modes

A μG can connect to the power grid through one or more PCCs or operate independently in islanding mode. The operational requirements vary depending on the situation, and there are differences in control and stability specifications. This flexibility allows the μG to adapt to different power needs and conditions, enhancing its utility and efficiency.

However, these variations also require tailored control strategies and stability measures for each operational mode [28]. Therefore, it is crucial to develop robust and adaptable systems to effectively manage these different scenarios.

2.2.1. Islanding Mode Operation of the Microgrid

The islanding operation mode of a μG occurs when a portion of the distribution grid is powered by one or more DGUs while the main grid is disconnected and isolated from the system. This "controlled island" mode significantly enhances the reliability of the EPS [29].

However, disconnection in systems with high DGU integration can lead to multiple power quality complications. Therefore, to maximize the benefits of DGUs, it is recommended to operate the μG in the "intentional island" mode [30]. The implementation of intentional islands is a future consideration for the smart grid, as per the IEEE-1547 standard [31]. For successful execution of this mode, it is crucial for the system to quickly identify grid disconnection as it happens, necessitating an efficient island detection algorithm. While operating in islanding mode, μGs must maintain a constant balance between generation and demand. In this context, information acquisition systems are vital for achieving optimal operation. Another important consideration in this type of μG operation is the disconnection from and subsequent reconnection to the electrical grid for synchronization reasons. The PCC must provide the facilities so that the μG can connect to the grid when necessary.

Table 1 shows the limits of the synchronization parameters according to the IEEE-1547 standard. Similarly, during islanding mode operation, the system ground must meet safety requirements and maintain impedances at acceptable levels. These considerations are established in the IEEE-1547 standard. This highlights the importance of adhering to these standards for safe and efficient operation of μGs.

Table 1. Synchronization parameters to reconnect the μG to the grid according to the IEEE-1547 standard [31].

Power of the DGUs (MVA)	Frequency Difference (Δf, %)	Voltage Difference (ΔV, %)	Angle Difference ($\Delta\Phi$, °)
0.0–0.5	0.3	10	20
>0.5–1.5	0.2	5	15
>1.5–10	0.1	3	10

2.2.2. Grid-Connected Mode Operation of the Microgrid

The μG is activated whenever a fault in the electrical grid is fixed. Before switching to the grid-connected mode, the μG voltage is synchronized with the grid's voltage. The μG aims to meet most of the demand, overseeing both the charging and discharging of the ESSs.

In this setup, the electrical grid serves as a balance bus, absorbing or delivering energy fluctuations. Also, the connection point acts as a reference for voltage and frequency, simplifying the maintenance of these parameters within the μG. In this scenario, it is not necessary for all the energy required by the loads to be generated solely by the μG's DGUs. The energy flowing through the PCC can offset any discrepancy between generation and consumption. Depending on whether the generation is greater or lesser than the energy demanded by the loads, the μG could be perceived as a smaller-scale generator or as a load. This operational approach has the advantage of being designed to reduce energy costs for associated consumers. It also optimizes the use of local generation when it is economically efficient, thereby reducing dependence on the electrical grid. Figure 5 illustrates a μG in both operation modes.

It is important to note that the successful implementation of these modes requires careful planning and control, as well as adherence to safety and quality standards. This includes promptly identifying grid disconnections, maintaining a constant balance between generation and demand, and ensuring safe and efficient disconnection and reconnection processes. These considerations highlight the complexity and sophistication of μG operations [32].

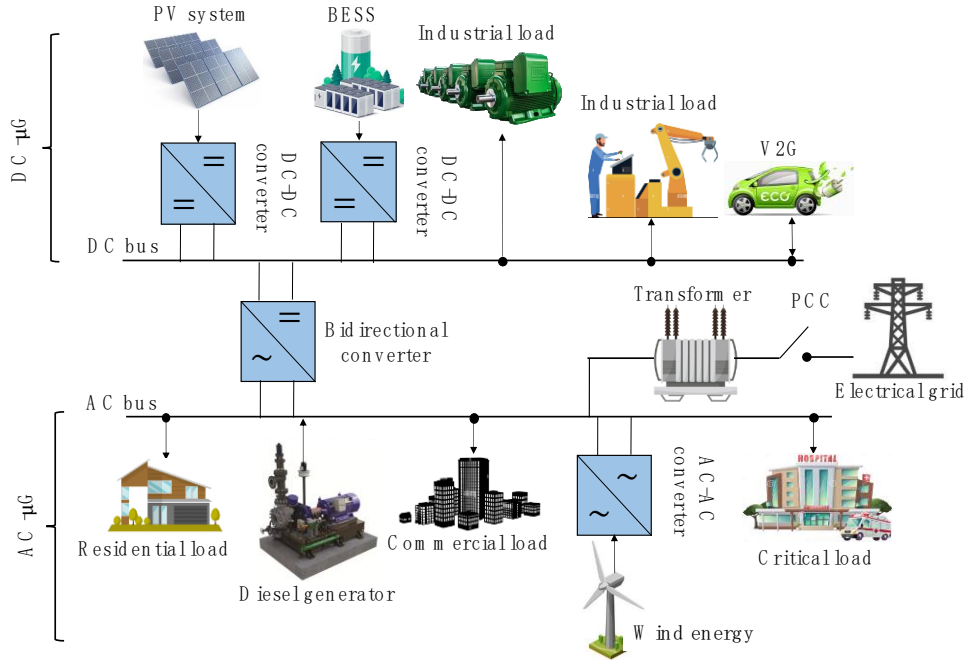

Figure 5. Operation modes of a hybrid microgrid.

2.3. Technical Aspects of Electrical Microgrids

This section provides a comprehensive overview of the technical aspects related to integration into the EPS.

2.3.1. Power and Voltage Unbalance

When the μG transitions from grid-connected mode to islanding mode, it generates power imbalance and voltage fluctuations. This could also be a result of the slow dynamic response and low inertia of DGUs. Voltage unbalance is a frequent occurrence in μGs. The magnitude of this imbalance in the system is evaluated by the Voltage Unbalance Factor (VUF). This scenario could lead to detrimental effects on power electronics and μG devices, as they may experience higher losses and reduced stability under unbalanced conditions. Therefore, it is crucial to limit the VUF by applying coherent criteria established in the grid codes, ensuring the stable and reliable integration of μGs [33]. For instance, the VUF is not permitted to exceed 3% according to the IEEE standard and 2% according to the IEC standard [34]. The Chinese, German, and London governments have imposed regulations that establish a maximum value of 2% [35]. Similarly, Canadian standards also establish a maximum value of 2% [36].

2.3.2. System Stability

Because of the diverse operational characteristics of μGs and DGUs, challenges to EPS stability arise. The main reasons for the stability problems are listed below:

- Decreased inertia of the system, resulting in frequency variations and angular instability;
- Low voltage stability due to more limited power distribution;
- Frequency fluctuations due to a change in the proportion of power sharing.

Decentralizing supply and maintaining an appropriate demand for the supply relationship can improve system stability [37].

2.3.3. Harmonic Distortion

The importance of power quality in μGs, both in islanding and grid-connected modes, is determined by the presence of non-linear and unbalanced loads, which constitute a significant portion of the system. These loads cause issues such as harmonic distortion, imbalances, and voltage variations in grids with limited capacity [7]. High impedances

in the system also generate harmonic distortion and voltage unbalance, compounded by problems in load distribution due to the variability of DGUs such as PV systems, wind turbines, and fuel cells.

Harmonic distortion threatens the power grid's ability to operate reliably and consistently if certain precautions are not taken. As a result, the safety of ESSs is compromised since they are more sensitive to harmonic distortion [38]. Therefore, harmonics of any order (preferably higher order) are eliminated and/or attenuated using active and/or passive filters [39].

Most EPSs have some capacity to tolerate harmonic distortion. However, an increase in harmonic distortion will undoubtedly cause line loss, overheating, communication failures, and activation of the protection switch [40].

Therefore, the issue of harmonic distortion must be minimized by μGs in accordance with current grid standards and codes [41]. The THDs, both voltage (THD_v) and current (THD_i), must be kept below 5% according to the IEEE-519 standard or IEC standards. For instance, THD_i must be 3% according to the United Kingdom (EREC G83) [42], and for THD_v, it should not exceed 5% in low and medium voltage according to IEEE or IEC standards [43]. Table 2 presents the current and voltage limits in terms of harmonics that must be achieved at the PCC.

Table 2. Current and voltage harmonic distortion limits of the μG [41–43].

Standards		Harmonic Order	Limit	THD
Current harmonics	IEEE-1547	$3 \leq h < 33$ (odd) $2 \leq h < 32$ (even)	$< (4\% - 0.3\%)$ $< (1\% - 0.5\%)$	<5%
	IEC 61000-3-2 [41]	$3 \leq h < 39$ (odd)	$< (0.3\% - 0.6\%)$	<5%
	UK (EREC G83 Stds.) [42]	$8 \leq h < 40$ (even) $3 \leq h < 35$ (odd) $8 \leq h < 40$ (even)	$< (0.2\% - 1.6\%)$ $< (2.3\% - 0.15\%)$ $< (0.23\% - 0.3\%)$	<3%
	GB/T ECM [35]	$1 \leq h < 33$ (odd) $2 \leq h < 30$ (even)	$< (4\% - 0.3\%)$ $< (1\% - 0.5\%)$	<5%
Standards		**Voltage Level**	**Harmonic Limit**	**THD**
Voltage harmonics	IEC	$(V > 161)$ kV $(69 \leq V \leq 161)$ kV $(2.3 \leq V \leq 69)$ kV	1% 1.5% 3%	1.5% 2.5% 5%
	IEEE-519	$(V > 161)$ kV $(69 \leq V \leq 161)$ kV $(1 \leq V \leq 69)$ kV $(V \leq 1)$ kV	1% 1.5% 3% 5%	1.5% 2.5% 5% 8%

The THD is indeed a crucial indicator used to quantify the harmonic content of a voltage or current signal. It is based on the relationship between two magnitudes: the effective value of the harmonic residue and the fundamental component. In essence, it provides a measure of the extent to which the signal deviates from a pure sinusoidal waveform due to the presence of harmonics. This makes it an essential tool for assessing power quality in EPSs.

Harmonic Distortion in μGs Operating in Grid-Connected Mode

Harmonic distortion is a common issue in this operation mode [10,44]. Many grid standards and codes now require new regulations for integrating DGUs. According to these regulations, DGUs must be disconnected from the power grid [45]. DGUs operating in grid-connected mode are listed in Table 3.

Table 3. Power quality issues in the DGUs that make up the μGs operating in grid-connected mode.

Power Quality Issue	PV	Wind Turbine	Hydro	Biomass	Diesel
Voltage sags	×	✓	✓	✓	✓
Voltage swells	×	✓	×	×	✓
Voltage unbalances	✓	×	×	✓	×
THD	✓	✓	✓	×	×
Interruptions	✓	✓	×	✓	×

Harmonic Distortion in μGs Operating in Islanding Mode

The interaction between loads, DGUs, and ESSs during μG transition states can have a negative impact on power quality when the μG operates in islanding mode. This reduces the impedance value of the μG, leading to significant voltage variations and an increased likelihood of generating high levels of harmonic distortion [46]. Even during islanding-mode operation, harmonic distortion remains a significant challenge for power quality in μGs. This issue encompasses not only the harmonics of the fundamental frequency but also the presence of inter-harmonics, sub-harmonics, and supra-harmonics. To tackle this problem, control strategies are implemented to reduce the THD index in μGs.

Additionally, another issue present in islanding-mode operation is voltage deviations, which occur due to the increase in harmonic voltage distortion resulting from resonances at low frequencies [47].

3. Model Description Proposed

This section offers a detailed overview of the proposed μG model for this study obtained from the IEEE 14-bus distribution system, which is a representation of a simple approximation of the US power system and it consists of 5 generators, 14 buses, and 11 loads. Data on loads, generators, buses, transformers, and lines were obtained from the standardized IEEE 14-bus data sheet. The base apparent power of this distribution system is 100 MVA and the data in tables are referenced based on this value. Figure 6a shows the original IEEE 14-bus distribution system, Figure 6b shows the proposed 14-bus μG after manually modeling the original system parameter, and Figure 6c shows MATLAB-Simulink® block diagram of the proposed model of the 14-bus μG system.

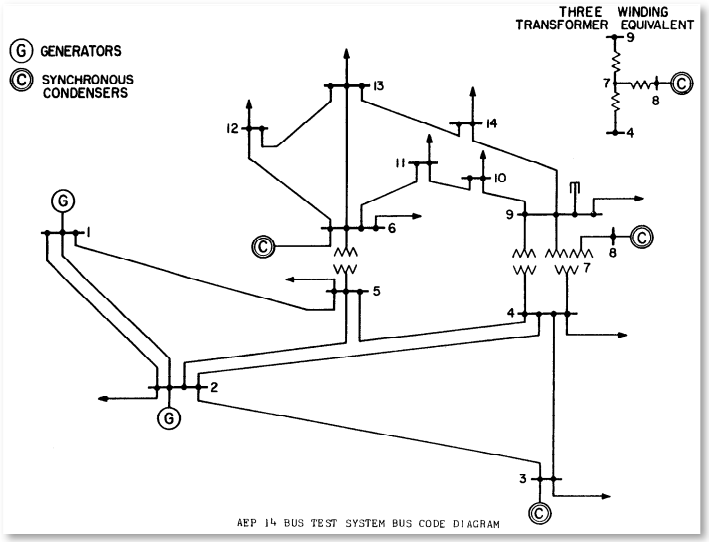

(**a**)

Figure 6. *Cont.*

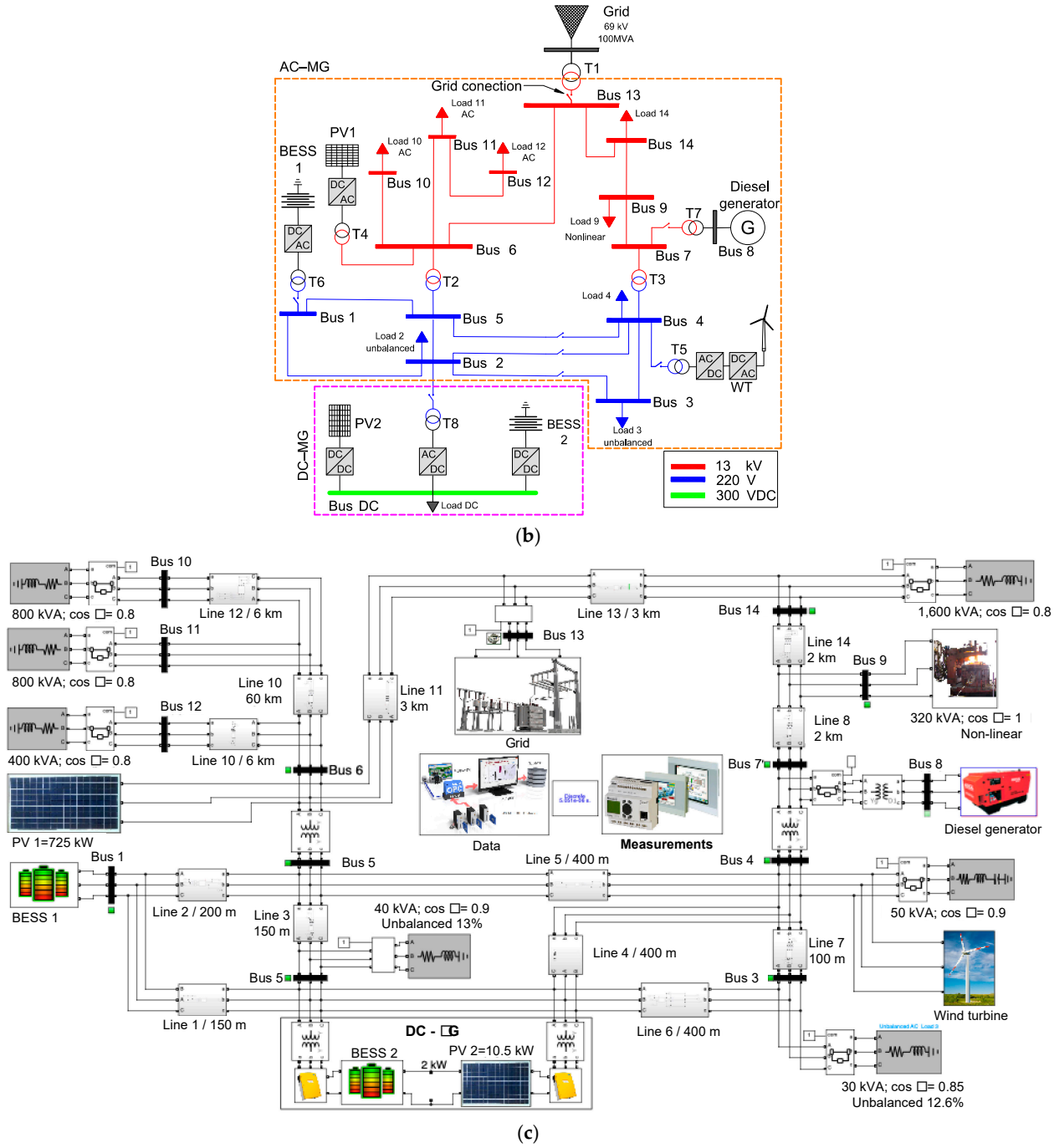

Figure 6. (**a**) Original IEEE 14-bus distribution system. (**b**) Proposed hybrid μG model. (**c**) MATLAB-Simulink® block diagram of the proposed model of the 14-bus μG system.

Furthermore, specific data were obtained and modeled accordingly in MATLAB-Simulink, which is specialized software, with the goal of providing the scientific community with a tool to better understand μG dynamics and performance across various operational scenarios. The μG model is divided into three main segments:

- AC-μG: Marked by an orange dotted line, this segment operates at two voltage levels—220 V and 13.8 kV—via distribution lines. It includes a 725 kW PV system, a 3 MW diesel generator, a 750 kW wind turbine, and a 96 kW and 345.6 MJ $BESS_1$. It also supports a variety of linear and non-linear loads as well as balanced and unbalanced loads. This μG functions at a 60 Hz frequency.

- DC-μG: Highlighted by a magenta dotted line, this segment contains a DC bus featuring 960 W and 3.5 MJ $BESS_2$ and a 10.5 kW PV system. It is connected to the AC-μG through two bidirectional, parallel PCs, enabling the transfer of active and reactive power via transformers.
- Finally, the AC-μG connects to the main electrical grid at bus 13. The grid is modeled by a Thevenin equivalent with a voltage of 69 kV, a capacity of 100 MVA, and an X/R ratio of 10.

The following section will provide an in-depth explanation of the components included in the hybrid μG model depicted in Figure 6b.

3.1. PV System

In the μG under study, the PV system is a key component of the distributed renewable energy resources. The model features two PV systems:

- PV_1: Connected to bus 6, it comprises over 1750 panels with a combined nominal power output of 725 kW. This system operates under standard test conditions with a total solar irradiance (G) of 1000 W/m² and a cell temperature of 25 °C.
- PV_2: Linked to bus 2 within the DC section of the μG, it consists of 42 panels that collectively produce a nominal power of 10.5 kW under the same irradiance and temperature conditions.

The primary parameters of these PV systems are used by MATLAB-Simulink® to simulate and analyze the performance of the solar panels. These parameters are detailed in Table 4, providing insights into the efficiency, output, and behavior of the PV systems within the μG framework.

Table 4. PV arrays for the μG.

PV System	I_{mpp}	P_{max}	v_{oc}	V_{mpp}	I_{cc}
1	8.6 A	250 W	37.4 V	30.7 V	8.6 A
2	5.7 A	414.8 W	85.3 V	73 V	6.1 A

I_{mmp} = maximum power point current; P_{max} = maximum power; v_{oc} = open-circuit voltage; V_{mpp} = voltage at maximum power point; I_{cc} = short-circuit current.

The PV_1 system utilizes a voltage-controlled step-up DC-DC converter, equipped with a 6000 μF capacitor operating at 300 V_{DC}. It employs a closed-loop PWM control strategy at a frequency of 5 kHz. On the other hand, the PV_2 system uses an open-loop sine PWM inverter. The modulation index (m) is set to 1 when the voltage is reduced from 480 V_{DC} to 250 V_{AC}.

3.2. Permant Magnet Synchronous Generator (PMSG)-Based Wind Turbine

In medium- and low-voltage μGs, variable-speed wind turbines are commonly used, particularly Permanent Magnet Synchronous Generators (PMSGs). PCs play a vital role in this setup, as they effectively decouple the electric generator from the grid to which it is connected. The model features a 750 kW PMSG wind turbine, operating at 575 V, linked to bus 4. MATLAB-Simulink® leverages the main parameters of the PMSG, which are listed in Table 5, to simulate and assess the generator's performance.

The wind turbine requires an AC-AC PC (commonly used back-to-back PC) to adjust the generator's parameters to match those of the electrical grid. The voltage and frequency of the wind turbine can be controlled using PWM control schemes for the PC and learning systems for the maximum power point tracker (MPPT).

Table 5. PMSG-based wind turbine parameters.

Parameter	Value
Power (P_m)	750 kW
Torque (T_m)	318 Kn × m
Voltage (V_s)	575 V
Current (I_s)	676 A
Frequency (f)	60 Hz
Pole Pairs	26
Speed	22.5 rpm
Stator resistance	6.5 mΩ
Rotor resistance	0.76 mΩ
Stator inductance	3.85 mH
Rotor inductance	1.12 mH
Magnetic flow	8.53 Wb
DC Capacitance	0.16 F
DC voltage	1220 V

3.3. BESS

The ESS is an integral part of the μG, enhancing the grid's adaptability during emergencies or when shifting to islanding mode. Among various ESS technologies, batteries are extensively employed in μG settings due to their established and recognized status as a mature technology. These systems store energy electrochemically, with an overall efficiency typically ranging from 60% to 80%, influenced by the operational cycle and the battery's electrochemical composition.

Batteries are differentiated by their structural characteristics and operational principles, encompassing types such as lithium-ion (Li-ion), lithium-polymer (Li-Poly) [48], lithium–iron phosphate (LiFePO4) [49], lead–acid (Pb-Acid), nickel–cadmium (Ni–Cd), nickel–metal hydride (Ni–MH) [50], nickel–zinc (Ni–Zn) [51], zinc–silver oxide (Zn–Ag), sodium–sulfur (NaS), ZEBRA [52], vanadium redox flow (VRF) [53], polysulfide–bromide (PSB), and iron-based flow batteries [54], among others. For μG applications, the primary battery-based ESSs include PbA, Ni-Fe, Ni-Cd, Ni–MH, and Li-ion batteries [55]. This study focuses on the last two types, chosen for their environmental advantages, life cycle comparable to that of lead–acid batteries, and their expanding capacities. Despite its premium cost, the Li-ion battery is also selected for its exceptional energy density.

The $BESS_2$ is linked to the DC bus and features a Li-ion battery with a nominal capacity of 800 Ah and a nominal voltage of 120 V_{DC}. In contrast, $BESS_1$ is connected to bus 1, housing three Ni–MH batteries, each with a nominal voltage from 650 V_{DC} to 900 V_{AC}. Battery parameters are time-varying and depend on the state of charge (see Table 6).

Table 6. BESSs for the μG proposed model.

	Battery Unit	Nominal Voltage	Rated Capacity	Initial SoC
$BESS_1$	Battery 1	120 V	800 Ah	80%
$BESS_2$	Battery 1	650 V	1.5 Ah	80%
	Battery 2	650 V	1.5 Ah	80%
	Battery 3	650 V	1.5 Ah	80%

3.4. PC

PCs are indispensable components within μGs due to their advanced technology, which enables a wide range of μG applications. These applications include the integration of renewable energy, electrification of transport systems, energy storage, and providing power supplies for computing needs. This study utilized two PC topologies: three-phase DC-DC converters and three-phase DC-AC converters.

The three-phase DC-DC converters are crucial for adjusting voltage levels between different DC sources and loads, while the three-phase DC-AC converters, or inverters, are essential for converting DC into AC power, facilitating the supply of electricity to AC-dependent systems and the broader AC grid.

3.4.1. DC-AC PCs

The PV_2 system is connected to the 13.8 kV AC system through an inverter that reduces the voltage from 480 V_{DC} to 250 V_{AC}. This inverter is designed with a three-level PWM-controlled Insulated-Gate Bipolar Transistor (IGBT) bridge. It operates using a closed-loop control strategy, complemented by a PWM carrier signal of 2 kHz. In addition, the $BESS_2$ is connected via a DC-DC converter to a 300 V_{DC} bus, which interacts with the 220 V system through an inverter that increases the nominal voltage from 650 V_{DC} to 900 V_{AC}. This inverter utilizes a multi-level topology, which is deemed the most efficient and reliable, as supported by the literature. It considers factors such as power losses, THD, and overall efficiency. Moreover, it uses an open-loop sinusoidal PWM (SPWM) method with a carrier frequency of 2.5 kHz. Importantly, on the AC side, the inverter produces a modulation index of 1.2.

3.4.2. DC-DC PCs

The PCs situated within the DC-µG are represented as a bidirectional DC-DC converter for the $BESS_1$, and as a DC-DC boost controller for the PV_1 system, as depicted in Figure 7. Their specifications are detailed in Table 7.

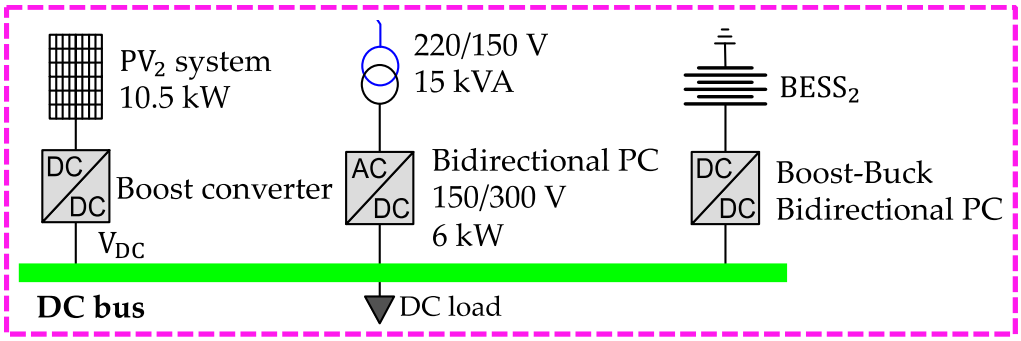

Figure 7. DC-µG.

Table 7. DC PC parameters.

DC Bus Power Converter	PWM Frequency	Capacitor	V_n (V_{DC})
Bidirectional boost–buck	5 kHz	1200 µF	300 V
Boost	5 kHz	1200 µF	300 V

Given the variable output voltages of the PV systems, which are inherently intermittent, it is crucial to link both PCs to the DC bus via a regulated DC-DC converter to stabilize the output voltage. In this research, a DC-DC boost converter was chosen to elevate the input DC voltage (V_i) from a range of 100–130 V to an output DC voltage (V_o) of 350 V. To mitigate electromagnetic interference and Eddy currents, the switching frequency was established at 5 kHz, with a capacitance of 1.2 kµF, inductance of 9 mH, and a DC resistance of 45 Ω. Furthermore, the $BESS_1$ charging and discharging cycles are managed by a bidirectional DC-DC controller, which connects the DC bus voltage with the battery system voltage. It is essential to note that two PI controllers are utilized to derive the reference current signal needed for the battery's charge and discharge processes. This approach aims to minimize current ripples, thereby enhancing efficiency and extending the operational lifespan of the BESSs. Notably, when the µG functions in island mode, the control strategy adjusts the DC bus voltage accordingly.

3.5. Power Transformers

This study examines seven power transformers. Among them, the substation transformer (T1) features a transformation ratio of 69 kV/13.8 kV, Δ-Y configuration, and an equivalent series impedance of 1.5% relative to its MVA base. This transformer facilitates the connection of the μG distribution system to the 69 kV sub-transmission system. Transformers T2 and T3 are designated for voltage conversion from 13.8 kV for industrial or commercial applications to 220 V for residential usage. Conversely, the PV system (T4), wind turbine (T5), $BESS_1$ (T6), and diesel generator (T7) are integrated with the μG through inverters. The specifications of these transformers are detailed in Table 8.

Table 8. Transformer parameters.

Transformer	P_{nom} (MVA)	Voltage Relationship (kV) (AV/BV)	R_{cc} (pu)	X_{cc} (pu)
T1	100	Yg 69/13.8 D1	0.015	0.015
T2	1.5	Y 13.8/0.22 Y	0.03	0.03
T3	1.5	Y 13.8/0.22 Y	0.03	0.03
T4	1	Yg 13.8/0.25 D1	0.0012	0.03
T5	1	Yg 13.8/0.25 D1	0.0012	0.03
T6	0.5	D1 0.9/0.22 Y	0.003	0.06
T7	3.5	Yg 13.8/2.4 D1	0.015	0.015

P_{nom} = rated power; R_{cc} = short-circuit resistance; X_{cc} = short-circuit reactance.

3.6. Loads

The electrical load is a critical factor in the design of an EPS due to its inherently unpredictable nature. This study accounts for a maximum demand scenario, which represents the highest power peak within a specific timeframe. The various types of loads involved are detailed in Table 9, summarizing the load data connected to the system. It is noteworthy that both balanced and unbalanced linear loads are modeled as constant impedances. Some loads include single-phase components that may disrupt the voltage and current symmetry of the system.

Table 9. Characteristics of the different types of loads.

Bus	Voltage	Load Type	kVA	PF	
2	Low voltage (LV)	Unbalanced	40	0.9	13
3	Low voltage (LV)	Unbalanced	30	0.85	12.6
4	Low voltage (LV)	Linear	15	0.9	–
9	Low voltage (LV)	Non-linear	320	1	–
10	Low voltage (LV)	Linear	800	0.8	–
11	Medium voltage (MV)	Linear	400	0.8	–
12	Medium voltage (MV)	Linear	800	0.8	–
14	Medium voltage (MV)	Linear	1600	0.8	–
DC	DC	DC load	2	1	–

In an ideal three-phase current distribution system, the load currents should be equal across all three phases. However, should an imbalance occur, it can lead to overloads and heating in power conductors, trigger protection mechanisms, and cause currents to flow through the grid's neutral wire. The degree of load imbalance is quantified by the maximum current deviation in any phase compared to the average load current. Reducing the unbalance index value, which can be achieved through various load balancing techniques, correlates with decreased power losses.

Non-Linear Loads

In this model, an electric arc furnace located at bus 9 is characterized as a non-linear load, as shown in Figure 6. Electric arc furnaces are known to produce considerable disturbances in μG applications. An electric arc furnace consists of a crucible or a steel shell lined with refractory material, filled with scrap metal, and equipped with three graphite electrodes. These electrodes are mounted on a movable support, which allows them to be adjusted up or down based on the control system's output. The various operational stages of electric arc furnaces—namely, start-up, melting, and refining—impact the voltage and current THD differently.

Fundamentally, a three-phase electric arc furnace can be represented as a variable resistor. Table 10 outlines the parameters of the electric arc furnace, which receives power directly from the 13.8 kV distribution grid.

Table 10. Non-linear load parameters.

PMW Freq.	Power	Capacitor	Rated Voltage	Resistance	Phi (°)
4080 Hz	320 kVA	10 μF	18,500 V_{AC}	1084 Ω	−30

3.7. Distribution Lines

This model incorporates two distribution levels, medium and low AC voltage, which are standard for μG applications. For the 13.8 kV primary grid, a 1/0 bare copper conductor was chosen, featuring a resistance of 0.394 Ω/km, a reactance of 0.1168 Ω/km, and an impedance of 0.411 Ω/km. For the 220 V secondary grid, a 4/0 copper TW cable was selected, with a resistance of 0.198 Ω/km, a reactance of 0.1089 Ω/km, and an impedance of 0.227 Ω/km. The specifics of the line sections utilized are presented in Table 11.

Table 11. Distribution line parameters.

Line	Output	Input	R (Ω)	X (Ω)	Distance
1	LV 1	LV 2	0.0297	0.016335	0.15 km
2	LV 1	LV 5	0.0396	0.02178	0.2 km
3	LV 2	LV 5	0.0297	0.016335	0.15 km
4	LV 2	LV 4	0.0792	0.04356	0.4 km
5	LV 4	LV 5	0.0792	0.04356	0.4 km
6	LV 2	LV 3	0.0792	0.04356	0.4 km
7	LV 3	LV 4	0.0198	0.01089	0.1 km
8	MV 7	MV 9	0.788	0.2336	2 km
9	MV 6	MV 11	2364	0.7008	6 km
10	MV 6	MV 12	2364	0.7008	6 km
11	MV 6	MV 13	1182	0.3504	3 km
12	MV 10	MV 11	2364	0.7008	6 km
13	MV 13	MV 14	1182	0.3504	3 km
14	MV 9	MV 14	0.788	0.2336	2 km

4. Analysis and Simulation of Hybrid μG

A hybrid μG connected to the electrical grid is the focus of this power quality case study. The total daily demand curve of the proposed μG is illustrated in Figure 8. It is derived from aggregating the hourly demands of each load within the model, with a primary emphasis on industrial and commercial loads. The loads are modeled as constant impedances, allowing for the identification of minor discrepancies between the nominal power of the load and the actual power consumption. Notably, the period of maximum demand occurs at 11:00 a.m. (see Figure 8a), aligning with the zenith of solar radiation. Consequently, this coincides with the peak generation potential of the PV systems. The surge in demand at this hour results from the amalgamation of industrial and residential load profiles.

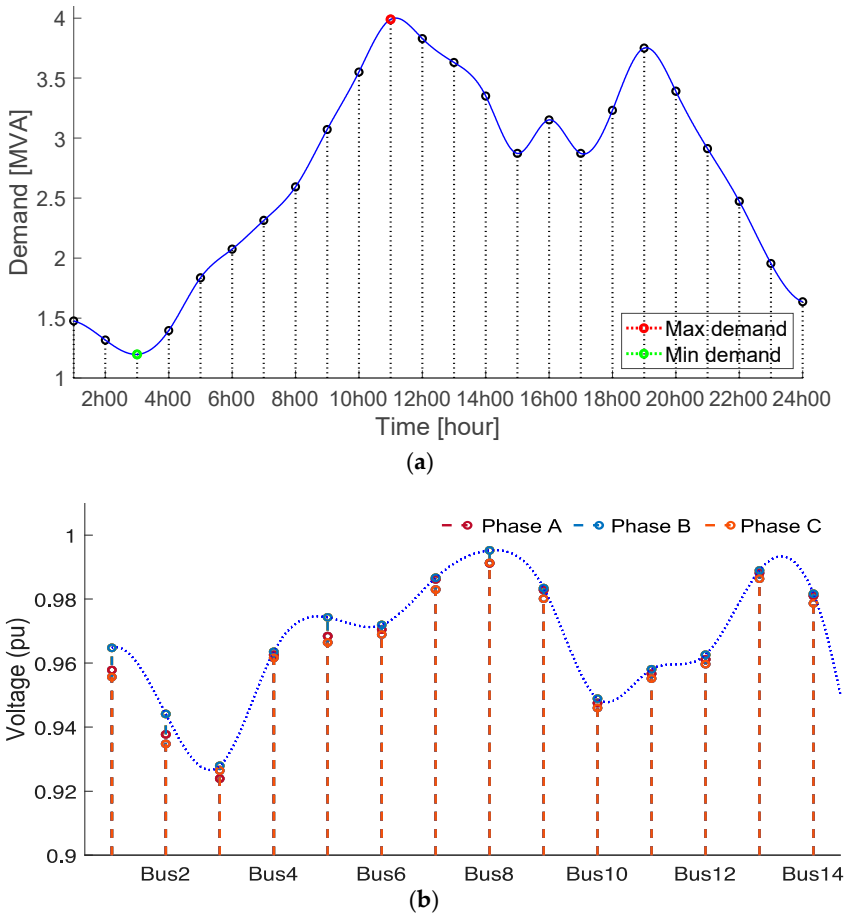

Figure 8. (**a**) Electrical energy demand curve. (**b**) Voltage profile.

4.1. Voltage Profile Analysis

One key power quality indicator for distribution system design is that the voltage delivered to consumers must remain within specific limits set by regulatory and control authorities. In Mexico, regulations stipulate that for distribution grids handling voltages above 1 kV and below 60 kV, the voltage variation should not exceed ±5% of the nominal voltage. The voltage profile of the proposed µG, which exhibits a voltage drop across various system sections, is depicted in Figure 8b. The voltage readings at each bus are enumerated in Table 12.

Table 12. Voltage profile of phase "A" in each of the buses of the µG.

Bus	PU	Bus	PU	Bus	PU	Bus	PU
1	0.955	5	0.967	9	0.975	13	0.985
2	0.942	6	0.971	10	0.946	14	0.981
3	0.939	7	0.983	11	0.959	-	
4	0.961	8	0.988	12	0.963	-	

The system experiences unbalanced loads due to the presence of single-phase load components. Although the voltage profile remains within acceptable operational limits, notable voltage sags are observed in the low-voltage (LV) grid (220 V) at buses 2, 3, and 10. Voltage sags must adhere to specific regulations for µG applications. For instance, according to the German standard, the µG is required to stay connected to the electrical grid and contribute reactive power to support the system, even if the voltage drops to 0% of its nominal value for 0.15 s; failure to do so necessitates disconnection. Similarly, in the event of voltage swells, the µG must maintain connection even if the voltage surges

to 120% of its nominal value for 0.1 s; otherwise, disconnection is compulsory [56]. These observations pave the way for future research aimed at finding solutions to enhance the voltage profile.

4.2. Power Factor (PF)

The conversion quality from AC to DC is gauged by specific performance metrics. Among these is the PF, which quantifies the ratio of power utilized by the electrical loads to the power supplied by DGUs and/or the conventional grid. Essentially, PF indicates the extent to which the power outputted by the DGU is utilized by the electrical loads. Therefore, the PF is the ratio between the apparent power (VA) and the real power (W). The power factor is determined at an instant one-half cycle (based on the fundamental frequency timing wave) after the initiation of current flow by determining the asymmetrical and symmetrical currents at this point. A lower PF suggests the presence of harmonic components within the line currents. The IEEE-1547 standard interconnection standard initially restricted small renewable generators from actively controlling the voltage at their point of connection, thereby constraining the operational PF. This restriction led to losses for utility companies and, consequently, increased operational costs. To address this, the IEEE-1547 standard underwent revisions, and the updated IEEE-1547 standard edition now permits small renewable generators to engage in voltage management along the feeder lines, provided they have the utility company's approval. Nonetheless, a significant number of inverters remain incapable of injecting reactive power into the load. The PF across each bus in the proposed μG is depicted in Figure 9, while the PF values for each bus are enumerated in Table 13.

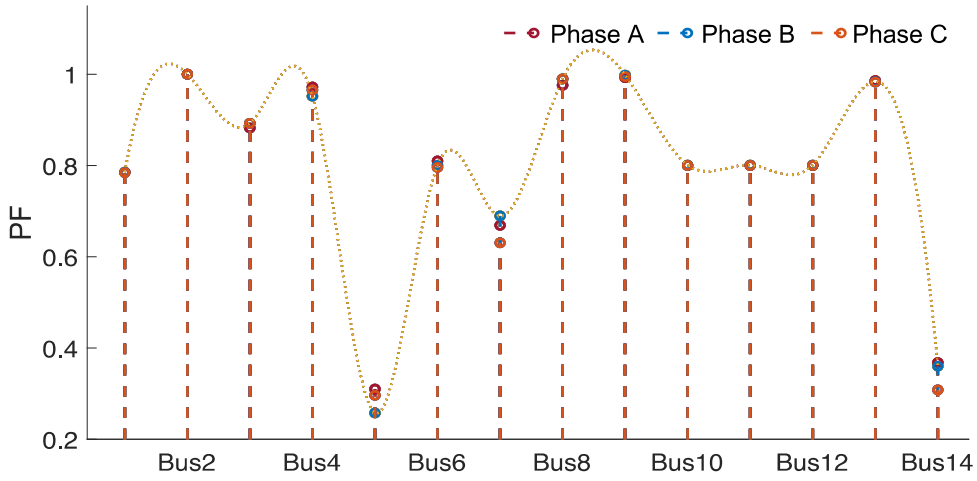

Figure 9. PF in each of the buses.

Table 13. PF of phase "A" in each of the buses of the μG.

Bus	PF	Bus	PF	Bus	PF	Bus	PF
1	0.8	5	0.38	9	1.0	13	1.0
2	1.0	6	0.84	10	0.85	14	0.4
3	0.9	7	0.7	11	0.85	-	
4	0.98	8	0.99	12	0.85	-	

Figure 9 illustrates that the PF at buses 2, 9, and 13 is nearly unified. This high PF at bus 2 arises from a singular active power input from the DC-μG. Similarly, the near-unified PF at bus 9 results from measurements taken directly at the connection point of the electric arc furnace. In contrast, buses 5 and 14 exhibit a significant decline in PF, attributed to their roles as power transfer buses where the transfer involves more reactive than active power. This decline is particularly pronounced at night due to the absence of solar radiation, which diminishes the active power contribution from PV systems.

The generation of harmonic components, which can disrupt the electrical grid's equipment—such as transformers, switches, and control systems—and cause voltage fluctuations, noise, and electrical disturbances like transients, is a primary consequence of a low PF. Moreover, this analysis reveals a potential conflict when attempting to compensate an EPS solely with active power. Such compensation leads to a degraded PF as perceived by the electrical grid, underscoring the necessity for a more comprehensive compensation strategy that incorporates both active and reactive power.

4.3. THD

To assess the harmonic content within a waveform, the THD metric is employed. This parameter evaluates the signal's quality or, alternatively, gauges the waveform's resemblance to an ideal sinusoidal shape. The THD can be utilized for analyzing both voltage and current waveforms. It is a crucial indicator for ensuring the fidelity of electrical signals in power systems.

4.3.1. Voltage THD

The voltage THD is defined as the relationship between the effective value of the total harmonic components and the effective value of the fundamental component. This indicator is used in high-, medium- and low-voltage systems. There are two ways to evaluate harmonic voltages: (i) individually, relating its relative amplitude V_k to the fundamental component of the effective voltage, "V_{ef}", and (ii) globally by calculating the voltage THD using the following expression [57]:

$$\mathrm{THD_v} = \sqrt[2]{\sum_{k=2}^{\infty}\left(\frac{{V_k}^2}{{V_{ef}}^2}\right)} \tag{1}$$

where "V_{ef}" is the effective value of the fundamental voltage wave and "V_k" is the effective value of the harmonic k. The recommended limit values for voltage harmonics are reflected in Table 14.

Table 14. Voltage distortion limits.

Bus Voltage at PCC	Distortion Harmonic	THD_v (%)
Less than 69 kV	3.0	5.0
69 kV to 161 kV	1.5	2.5
Greater than 161 kV	1.0	1.5

Figure 10 presents the voltage THD index for each bus within the system. The THD for each bus is computed as indicated in Equation (1). Additionally, Table 15 enumerates the magnitude (expressed in percentage) of the voltage THD for phase "A" at each of the µG buses. These data are essential for analyzing the power quality and ensuring the reliability of the electrical system.

Table 15. Voltage THD of phase "A" in each of the buses of the µG.

Bus	THD	Bus	THD	Bus	THD	Bus	THD
1	10.8	5	9.1	9	12.7	13	10.7
2	17.6	6	9.1	10	10.1	14	11.8
3	13.3	7	13.5	11	10.2	-	
4	14.8	8	13.2	12	10.3	-	

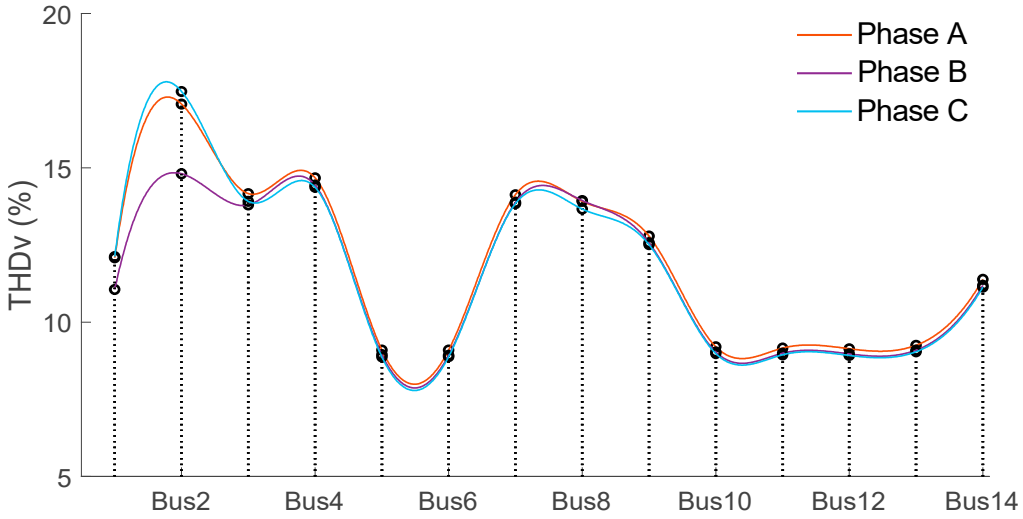

Figure 10. Voltage THD in each of the buses of the proposed μG.

As depicted in Figures 11–14, the voltage THD exceeds the permissible voltage distortion threshold of 5% as stipulated by the IEEE-519 standard (refer to Table 14). This non-compliance is attributed to the integration of substantial non-linear loads, such as the electric arc furnace, and the involvement of sizable variable DGUs, like wind turbines, which significantly influence the μG's performance. The three-phase voltage waveforms, along with the corresponding data for each bus, are detailed in Figures 11–14. This information is crucial for understanding the power quality issues and the operational challenges within the μG.

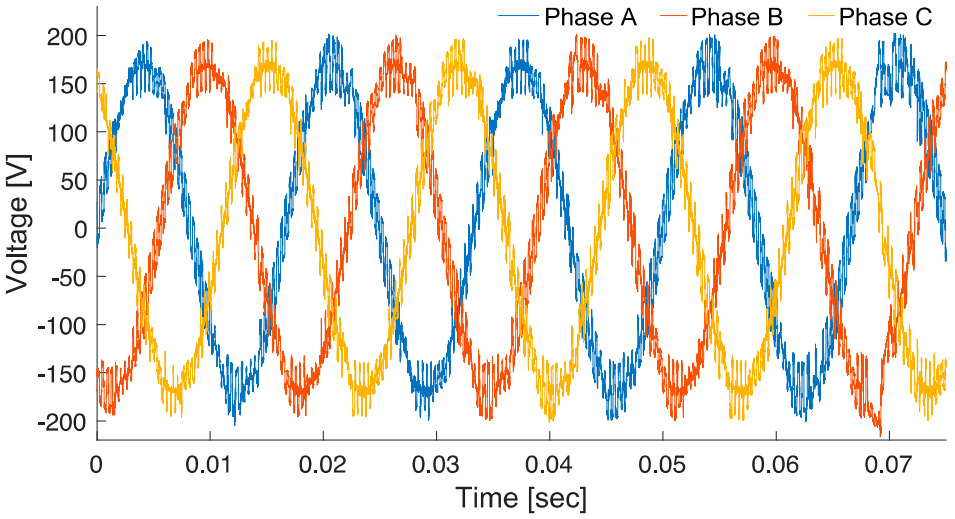

Figure 11. Three–phase voltage at bus 4.

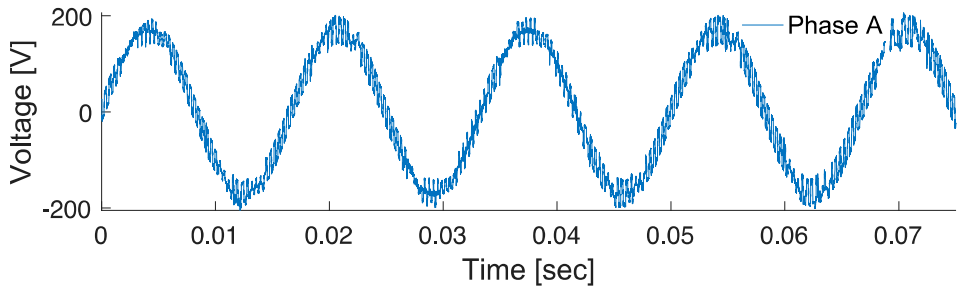

Figure 12. Phase "A" voltage at bus 4.

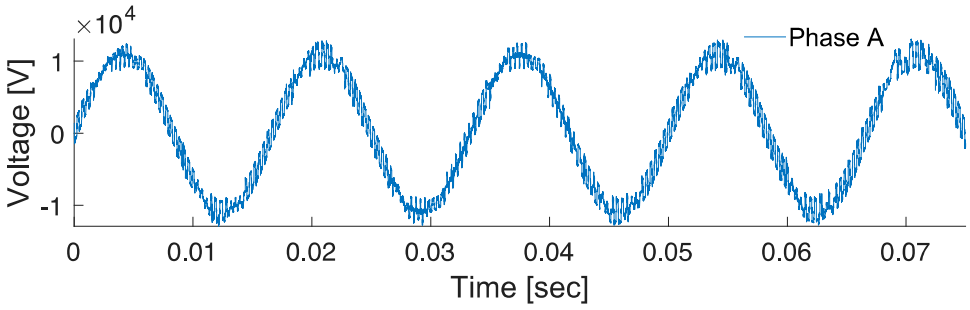

Figure 13. Phase "A" voltage at bus 7.

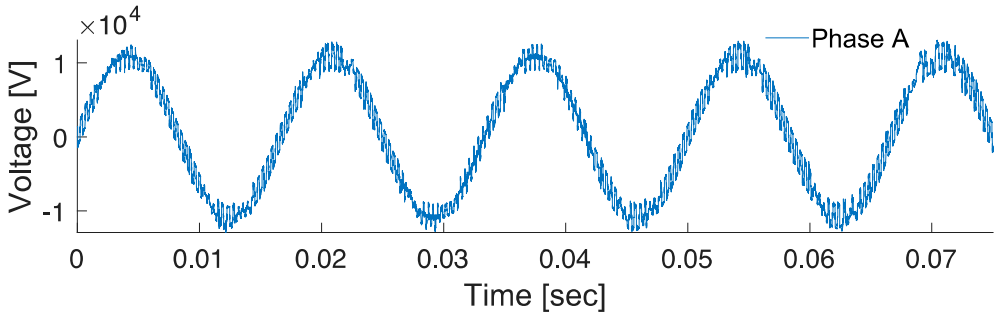

Figure 14. Phase "A" voltage at bus 9.

4.3.2. Current THD

THD is a significant factor that impacts power quality, particularly in distribution systems. To calculate THD for a current signal, both the harmonic currents and the fundamental harmonic are considered. THD values can range from a minimal percentage to values exceeding 100%, which is often the case with switched-mode power supplies. The calculation of THD is performed using Equation (2), as cited in reference [58]:

$$\mathrm{THD_i} = \sqrt[2]{\sum_{k=2}^{\infty}\left(\frac{{I_k}^2}{{I_{ef}}^2}\right)} \tag{2}$$

where "I_{ef}" is the effective value of the fundamental current wave and "I_k" is the effective value of the harmonic k. Table 16 lists the maximum limits expressed in % of the $\mathrm{THD_i}$ for different voltage levels in distribution systems. Figure 15 shows the current THD index for each of the system buses. The THD at each bus is calculated as shown in (2). Many harmonic current signals are generated in the bus where the non-linear load (electric arc furnace) is connected, as seen in Figure 15. Table 17 lists the magnitude (%) of the current THD of phase "A" in each of the μG buses.

Table 16. Maximum limits (%) of harmonic current distortion for distribution system (120 V–69 kV).

$\frac{I_{sc}}{I_d}$	$n < 11$	$11 \leq n < 17$	$17 \leq n < 23$	$35 \leq n$	THD
<20	4.0	2.0	1.5	0.6	5%
20 < 50	7.0	3.5	2.5	1.0	8%
50 < 100	10.0	4.5	4.0	1.5	12%
100 < 1000	12.0	5.5	5.0	2.0	15%
>1000	15.0	7.0	6.0	2.5	20%

I_{sc} = short-circuit current; I_d = demand current.

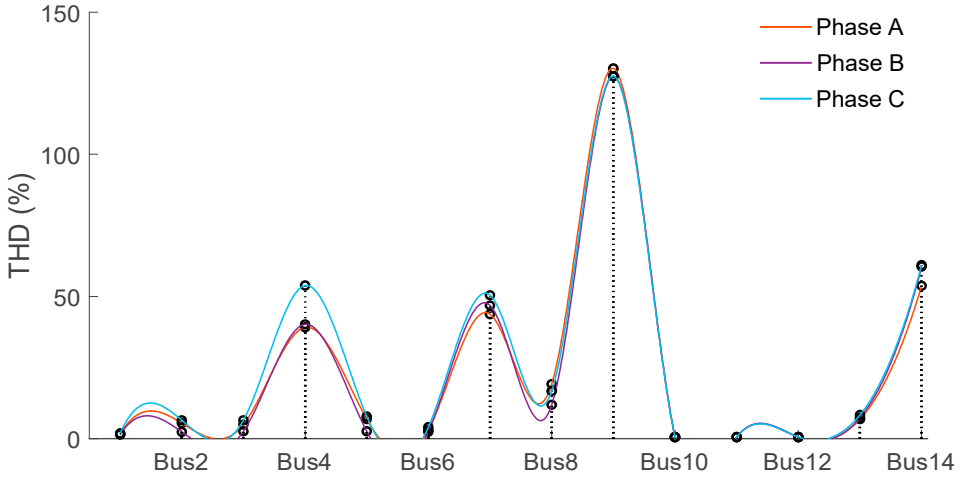

Figure 15. Current THD in each of the buses of the proposed μG.

Table 17. Current THD of phase "A" in each of the buses of the μG.

Bus	THD	Bus	THD	Bus	THD	Bus	THD
1	2.3	5	2.8	9	132.5	13	8.7
2	3.6	6	2.7	10	1.6	14	62.3
3	2.9	7	55.2	11	1.4	-	
4	46.7	8	23.8	12	1.5	-	

The fluctuations in the electric arc furnace's length led to erratic variations in the system's current, resulting in voltage changes that are proportional to the upstream impedance of the electric arc furnace. During start-up and scrap melting, the emission of harmonic currents at the system buses is notably high. Consequently, μGs are required to mitigate harmonic current emissions to comply with established standards and new regulations set forth by grid codes. The individual THD_i must remain below 5% as per general standards [42], while the UK standards (EREC G83) impose a more rigorous requirement of THD_i less than 3% [58].

The situation deteriorates with the detection of supra-harmonics, which arise from the proliferation of power electronic devices. These devices, such as PV system PCs, wind systems, power line communication systems, and electric vehicle chargers, are primary contributors to supra-harmonics in the electrical grid, generating high-frequency noise above 2 kHz. Currently, there are no established regulations concerning supra-harmonics.

To alleviate these issues, methods like reactive power compensation or the installation of capacitor banks are recommended. Another solution could involve increasing the short-circuit power at the PCC from 100 to 110 MVA, which is viable only if supplied from a higher voltage level, such as 13.8 kV. The choice between these solutions hinges on the project's economic viability and technical feasibility.

If the harmonic current emissions are not addressed promptly, additional problems may ensue, including the overheating of the neutral wire in three-phase systems, discrepancies in the secondary winding voltage of distribution transformers, and consequently, elevated copper and heat losses in electrical equipment. These issues are symptomatic of excessive harmonic distortion in systems with such characteristics.

Figure 16 displays the three-phase currents at bus 4, while Figures 17–19 present the single-phase current waveforms for the most vulnerable buses, as identified in Figure 15.

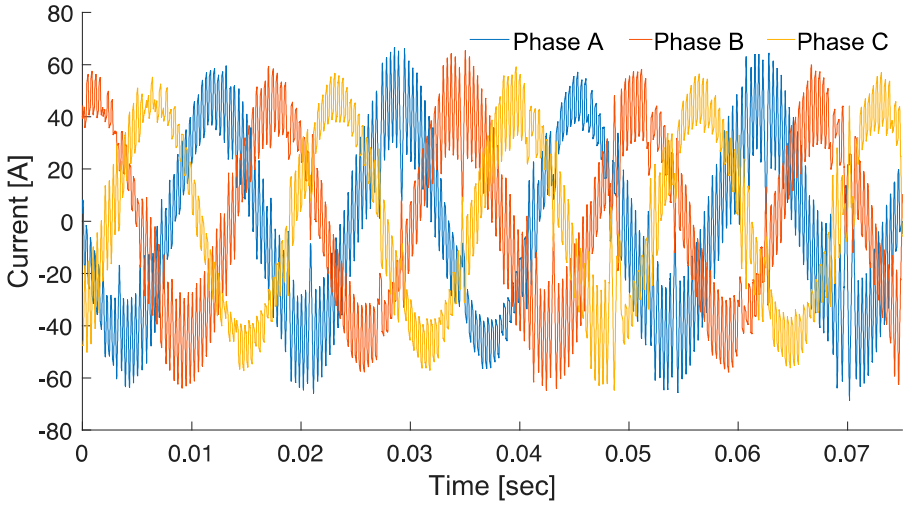

Figure 16. Three–phase currents at bus 4.

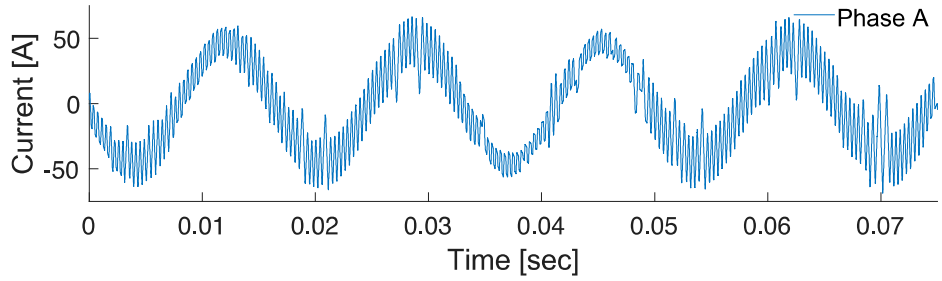

Figure 17. Current at bus 4.

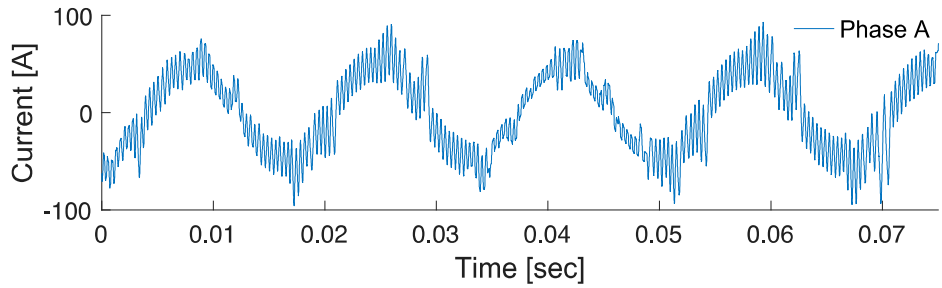

Figure 18. Current at bus 7.

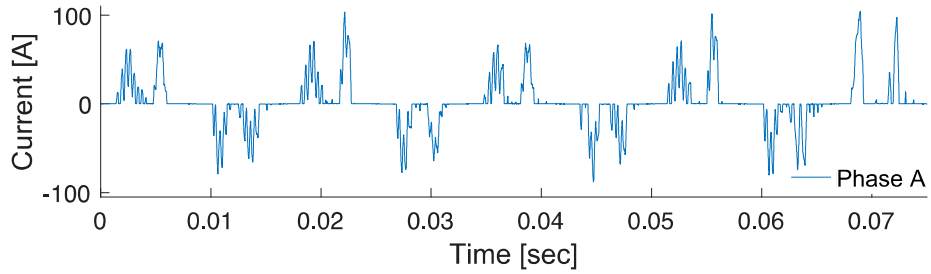

Figure 19. Current at bus 9.

The predominant harmonic components of the currents depicted in Figures 17–19 are enumerated in Table 18. It is crucial to acknowledge that the voltage and current harbor not only harmonic components but also inter-harmonic elements. These inter-harmonics are introduced by PCs due to their dual-frequency direct connections to the electrical grid.

Table 18. Harmonic currents components at buses 4, 7 and 9.

Bus	Sequence	Magnitude (%)	Angle (°)	Frequency (Hz)
4	0	10.25	148.2	180
	−	5.62	152.2	300
	+	2.50	−65.6	420
	0	4.86	45.3	540
	−	4.18	47.3	663.2
	+	8.17	−24.9	780
	−	6.33	64.4	840
	+	7.40	97.1	1145.2
	−	7.07	−37.9	1200
	+	9.66	40.1	1320.3
	0	6.55	−93.1	1440
	−	4.06	250.3	1562.9
	+	3.08	−110.4	1620
7	−	18.54	11.1	300
	+	7.49	121.6	420
	0	6.42	−29.4	540
	−	6.05	206.3	673.2
	+	4.94	222.9	784.6
	−	3.71	−255.7	840
	+	3.0	125	961.3
	−	6.26	−245.9	1020
	+	6.44	−57.6	1140
	0	2.83	27.0	1260
	−	4.18	−168.1	1382.6
	+	4.94	183.0	1500
	0	4.15	246	1620
9	−	84.98	27.0	300
	+	54.09	144.5	420
	0	19.23	−77.1	540
	−	38.67	−191.9	693
	+	6.43	85.8	781
	−	7.05	163.1	856.3
	+	4.27	−151.9	960
	−	14.06	48.7	1022.4
	+	11.8	−234.8	1320
	−	15.87	21.2	1579
	+	9.47	−237.9	1684.5

5. Discussion

The findings of this research derive from the design of a hybrid μG, comprising both an AC-μG and a DC-μG, each with a capacity of 4 MW. This design incorporates DGUs to facilitate power quality studies, focusing on voltage profile aspects such as unbalances, fluctuations, and sags, as well as PF and current and voltage THD. These findings are juxtaposed with the research detailed in references [14,17,22–24,59], as previously discussed in the literature.

Power quality assessment in an EPS typically revolves around the analysis of the voltage profile, which includes examining variations in voltage magnitude, flicker severity, voltage unbalance, and rapid changes like voltage sags, transient swells, and interruptions.

Reference [14] explores the voltage profile characteristics of a hybrid μG, analyzing data in 10 min aggregation intervals at the LV supply terminal. The μG in question integrates a 189 kW PV system, two BESSs of 200 kWh and 250 kWh, and a 45.5 kWp micro-PV system, catering to a demand of 1535.7 kW.

Statistical analysis was performed for each phase, considering parameters such as the minimum, maximum, mean, median, standard deviation, and the first and third quantiles, ensuring compliance with the IEC 61000-4-30 standards [42]. These results stem from

an initial scenario before connecting to the μG. Post-connection, however, the measured parameters at the test point exhibited significant variations, mirroring the current study's findings. This variability is attributed to the μG's composition, predominantly featuring different DGUs like PV and wind systems, which often incorporate advanced power electronics technologies that can introduce additional power quality issues.

As for the PF results at the buses of our research listed in Table 13, buses 5 and 14 display PF values significantly below the permissible limits set by the IEEE-519 standard. A similar observation was made in reference [17], where the authors deduced that maintaining a unitary PF across all buses of a hybrid μG connected to the electrical grid does not guarantee minimized energy losses and generation costs. Instead, optimizing the operating cost may be achieved by balancing positive and negative reactive powers across various μG buses. In line with IEC 60831-2 standard [60], maintaining the PF at or above 0.95 is essential for the system's efficiency, achievable through the deployment of intelligent controllers adept at reactive power control and compensation.

Continuing with this analysis, in this research, the observed voltage and current THD surpassed the limits recommended by the IEEE-519 standard. This was similarly noted in the study referenced in [59], which assessed the THD in a μG under varying degrees of PV penetration—30%, 50%, 70%, and 100%—relative to the total linear load at bus 7 of the LV grid, the non-linear load at bus 9, and a combined load (linear and non-linear) at bus 10. The study deduced that the THD indices breach the permissible threshold when the PV system's renewable penetration reaches 100%, injecting the entirety of the energy into the system. The results unequivocally demonstrate that both voltage and current THD escalate with increased levels of renewable penetration. This escalation is attributed to the aggregate impact of harmonic currents injected by PV inverters, particularly during peak PV generation, in relation to the full load current of the linear load at any LV-connected bus. Notably, the study did not incorporate any harmonic filters (neither passive nor active) within the μG; it solely considered the standard current harmonic data for each inverter and the non-linear load.

Like the authors in [59], a study developed in 2024 by Pontificia Universidad Católica Madre y Maestra [22] demonstrated that the THD_i obtained in the PCC of the μG increases as PV penetration increases. The work is developed under two different scenarios: the first scenario consists of a μG based on PV systems, BESS and programmable loads. The μG operates in connection with the electrical grid. The second scenario contemplates the use of the harmonic compensation technique with resonant filters. In order to compare the results obtained in this research with those published in [20], only the results of the first scenario are considered, where the THD_i of phase A of the grid current was measured when there were no disturbances in the electrical grid, which resulted in a THD_i = 7.27% in the grid current in phase A. In this case study, the authors considered programmable loads to which harmonic pollution was applied (5, 7, 11, 13 and 17). These voltage harmonics were applied to the 3∅ voltages of the grid, resulting in a THD_v = 33.54%. Therefore, the authors conclude that these values do not comply with international standards on harmonic distortion.

A similar study was developed in the μG laboratory of the University of Almería (Spain) [23]. The main elements of the μG are two PV systems of 3.6 kW each, three wind turbines and a BESS for subsequent use. The loads are static and for household appliance use. The μG is connected to the grid. The focus of the study is to analyze the power quality aspects such as voltage, current, power (active, reactive, apparent), PF, harmonics in voltage and current up to the 50th order, voltage and current THD, and frequency, among other parameters. Considering only the PF and THD as power quality aspects of interest in this study, it is concluded that the maximum values of the voltage THD range between 2.30 and 2.50%, which are permissible values according to international standards, while the current THD reaches maximum values of 58.70%, which indicates that it is outside the permissible limits. This is due to high solar penetration into the system's vulnerable loads. On the other hand, the minimum PF found in the study was 0.2 due to the activation of reactive

loads (inductive or capacitive). This same behavior occurs in the μG model proposed by our research. As renewable injection increases, current THD levels increase, making buses that are furthest from the PV system vulnerable.

Additionally, a study developed by Clemson University in the USA [24] highlights the impact of PV systems on an electrical μG considering linear/non-linear composite loads using the cross-frequency admittance matrix method. In that study, the following power quality aspects were analyzed: harmonic distortion, waveform distortion and system imbalance. The μG consists of four main loads: The first load considers a small-scale factory made up of a large number of motors and heating pumps connected on bus 51. The second and third loads consider two commercial buildings connected on bus 60 and 61, respectively; the last load is residential and connected on bus 62. The results of this research conclude that loads connected to bus 51 (motors, heating pumps and other heavy-duty non-linear loads) do not consume large amounts of energy, but still have the worst impact on the current waveform. For that reason, the research results are based on the measurement of currents because voltage distortion is not dominant. Regarding the results of the current THD, values of 25.87, 12.64 and 10.23% were obtained, which exceed the permissible limits by international standards. This is due to the compound loads connected to the vulnerable buses of the μG. Therefore, the authors determine that the contribution of harmonics from the PV inverter, the different types of non-linear loads in each phase and the system configuration significantly unbalance the μG. These conclusions are similar to the conclusions obtained in this work, where the THD levels of currents increased as the penetration of DGUs such as PV and wind increases. The same occurs when the non-linear load of the system (electric arc furnace) was located in vulnerable buses of the μG, which means an important contribution of harmonics injected into the system.

Table 19 summarizes the most important characteristics of the studies carried out around this research, with the aim of comparing the most important findings obtained in each study.

Table 19. Comparative studies on power quality issues in electrical μGs.

Aspects	Ostrowska, Anna et al. (2022) [14]	Raghavendra, L. (2023) [17]	Guerrero-Rodríguez N.F. (2024) [22]	Isanbaev Viktor et al. (2024) [23]	Zhanhe, Liu et al. (2015) [24]	This Paper
Characteristics of the proposed model						
PV system	PV power plant = 189 kW PV microinstallation = 45.5 kWp	11 kV, 200 kW	11 kWp/460 kW Temperature = 25 °C Irradiance = 1 kW/m^2	2 solar tracker systems with 3600 W capacity each	600 kW Irradiance = 1 kW/m^2	10.5 kW μG-DC and 750 kW μG-AC Temperature of 25 °C Irradiance = 1 kW/m^2
Power converter	×	DC-AC power converter	Dual 3∅ VSI 8 A, 800 $V_{DC-link}$. F-PWM = 35 kHz	×	DC-DC boost converter, 1 kHz, 300 V and 3∅inverter of 1 MW, 720 V_{DC}/300V_{AC}	Inverter operates using a closed-loop control strategy, with an F-PWM = 2 kHz.
ESS	200 kW, 250 kWh Li-ion battery	×	5 kWh lithium battery	2.6 kWh lithium battery	×	Li − ion battery = 800 Ah, 120 $V_{DC-link}$ Ni-MH battery = 1.5 Ah, 900 V_{AC}
Wind turbine	×	11 kV, 250 kW	×	3 wind turbines	×	750 kW PMSG-based wind turbine at 575 V.
Diesel generator	110 kVA	11 kV, 100 kVA	×	×	×	3 MW
Type of load	Total load capacity = 1535.7 kW	Active load = 435 kW Reactive load = 400 kVAR	Programmable, consisting of five 3∅resistive loads in a Y shape	Several home appliances: fridges, refrigerators, ovens, electronic devices, etc.	Bus 51 ≈ 80 kW Buses 60 and 61 ≈ 164.5 and 97.7 kW, and bus 62 ≈ 72 kW	Unbalanced (40 and 30 kVA), linear (800, 400 kVA), and non-linear (320 kVA)
Operation mode	Grid-connected μG	Grid-connected μG	Grid-connected μG	Grid-connected μG	Grid-connected μG	Grid-connected μG
Transformer characteristics in PCC	21/0.42 kV; 630 kVA	×	208Δ/208Y	×	1 MVA, 60 Hz, 300 V/4.16 kV	100 MVA, Yg 69/13.8 kV D1
Results of the investigation						
Voltage profile	Authors do not analyze it	Authors do not analyze it	Lower voltage profiles (in pu) at Bus 10 = 0.9486, bus 11 = 0.9478 and bus 12 = 0.9476.	Voltages on each bus are in the acceptable fluctuation range (0.95–1.05 pu)	Voltage in phase L1 = 226.4, 2.6% above nominal value	Notable voltage sags are observed in the LV grid at buses 2 (0.942), 3 (0.939), and 10 (0.946)
PF	An internal control loop regulates the generator PF ≈ 0.98	Minimum PF = 0.2 (due to the activation of reactive loads) Maximum PF = 0.98	Authors do not analyze it	Authors do not analyze it	Authors do not analyze it	Minimum PF = 0.38 in bus 5 exhibits a significant decline due to non-linear load presence
Voltage and current THD	THD_v = 33.54%, THD_i = 7.27% both at phase 1, without harmonic compensator	Maximum THD_v = 1.87%, and maximum THD_i = 11.56%	Maximum THD_v = 1.02% at bus 12, and maximum THD_i = 15.33% at bus 11	Maximum THD_i = 25.8, 12.64 and 10.23% at bus 51, 60 and 62. Voltage distortion is not dominant	Maximum THD_v = 2.21%, and maximum THD_i = 21.90%	Maximum THD_v = 17.6% at bus 2, and maximum THD_i = 132.5% at bus 9

6. Conclusions

The significance of power quality in μGs has escalated as a focal point of contemporary research within smart grids and power distribution grids. This investigation introduces a 4 MW hybrid μG model dedicated to power quality analysis. The model incorporates DGUs such PV systems and wind systems, contributing 25% power injection, alongside a traditional generation system providing the remaining 75%. It also accounts for both linear and non-linear loads, whether balanced or unbalanced, in addition to two BESSs. The μG model, designed to function in a grid-connected mode, was simulated using MATLAB-Simulink®. The outcomes were corroborated against the IEEE-519 standard's compatibility benchmarks, as delineated in Tables 14 and 16. The pivotal findings of this research are summarized below.

This study identifies three primary factors contributing to power quality challenges in μGs: (i) micro-sources, stemming from the erratic output of DGUs like PV systems and wind turbines; (ii) the utilization of power electronics within the μG; and (iii) diverse load types leading to increased demands for reactive power. The simulation results indicate that fluctuations in renewable energy production directly influence the dynamics of energy flow across the electrical grid and the diesel generator during grid-connected operations of the μG.

Variations in solar and wind resources precipitate changes in active power generation, thereby disrupting reactive power distribution. This disruption manifests as local voltage fluctuations at the μG's susceptible buses. Notably, the voltage profiles at buses 2, 3, and 10 were observed to be marginally low, registering at 0.94, 0.93, and 0.94 per unit (pu), respectively. Such discrepancies are attributed to the disproportionate allocation of single-phase loads and renewable sources, particularly PV systems and wind turbines. Moreover, substantial reductions in renewable energy input within a frail grid or during peak load conditions with LV can exacerbate these voltage fluctuations, potentially impacting sensitive equipment connected to these affected buses.

PF readings at buses 5 and 14 were recorded at 0.38 and 0.4, respectively, indicating a markedly low PF by IEEE-519 and IEC 61000-2 standards [42]. This occurs when real power (kW) diminishes while reactive power (kVArs) remains unchanged, resulting in a reduced PF. Consequently, it is imperative to distinguish reactive power flow from the PF metric, as the latter can fluctuate with proximate generation sources. Conversely, this study reveals that buses 2, 9, and 13 exhibit a unitary PF, suggesting that a high PF does not inherently reduce energy losses or generation costs. However, a strategic amalgamation of positive and negative reactive powers could optimize operational expenses.

The THD analysis concluded that voltage THD levels exceed the IEEE-519 standard's tolerance across all μG buses. Specifically, the current THD level at bus 14 peaked at 62.3%, well above the prescribed limit. Buses 4, 7, 8, 9, and 14 also reported current THD values of 46.7%, 55.2%, 23.8%, and 132.5%, respectively, surpassing acceptable thresholds. When operating in grid-connected mode, the μG's current THD percentage can be mitigated through the deployment of active harmonic filters, such as tuning filters, double-tuning filters, high-pass filters, and type C high-pass filters.

The insights gleaned from this research will inform the development of a hybrid μG model with enhanced operational conditions through the implementation of suitable control strategies. Building on these findings, forthcoming studies will concentrate on two main objectives: (i) integrating BESSs with reactive power compensation techniques, and (ii) formulating and applying optimal control and operational methodologies.

Author Contributions: E.H.-M.: Conceptualization, methodology, investigation, writing—original draft preparation, writing—review and editing, project administration.; C.R.J.-R.: investigation, supervision and writing—original draft.; J.A.E.-S.: conceptualization and visualization; A.L.-L.: conceptualization and visualization; R.A.G.-D.: visualization; J.A.R.-T.: visualization; J.D.R.-R.: visualization; O.A.J.: investigation and writing—original draft. All authors have read and agreed to the published version of the manuscript.

Funding: This research received no external funding.

Data Availability Statement: This item is where all data has to be shared due to copyright reasons.

Conflicts of Interest: We, the authors, declare that we have no conflicts of interest in the conduct of this research article.

Nomenclature

DGU	Distributed Generation Unit
μG	Microgrid
ESS	Energy Storage System
PF	Power factor
PV	Photovoltaic
BESS	Battery Energy Storage System
THD	Total Harmonic Distortion
PCC	Point of Common Coupling
PC	Power Converter
DC-μG	Direct Current Microgrid
AC-μG	Altern Current Microgrid
EPS	Electrical Power System
HVDC	High-Voltage Direct Current
VUF	Voltage Unbalance Factor
PWM	Pulse Width Modulation
PMSG	Permanent Magnet Synchronous Generator
MPPT	Maximum Power Point Tracker
IGBT	Insulated-Gate Bipolar Transistor
SPWM	Sinusoidal Pulse Width Modulation
THD_v	Voltage Total Harmonic Distortion
THD_i	Current Total Harmonic Distortion

References

1. Li, Y.; Feng, B.; Li, G.; Qi, J.; Zhao, D.; Mu, Y. Optimal distributed generation planning in active distribution networks considering integration of energy storage. *Appl. Energy* **2018**, *210*, 1073–1081. [CrossRef]
2. Ali, Z.M.; Calasan, M.; Abdel-Aleem, S.H.E.; Jurado, F.; Gandoman, F.H. Applications of energy storage systems in enhancing energy management and access in microgrids: A review. *Energies* **2023**, *16*, 5930. [CrossRef]
3. Planas, E.; Andreu, J.; Garate, J.I.; Martínez, I.; Ibarra, E. AC and DC technology in microgrids: A review. *Renew. Sustain. Energy* **2015**, *43*, 726–749. [CrossRef]
4. Sarwar, S.; Kirli, D.; Merlin, M.M.C.; Kiprakis, A.E. Major Challenges towards energy management and power sharing in a hybrid AC/DC microgrid: A review. *Energies* **2022**, *15*, 8851. [CrossRef]
5. Parhizi, S.; Lotfi, H.; Khodaei, A.; Bahramirad, S. State of the art in research on microgrids: A review. *IEEE Access* **2015**, *3*, 890–925. [CrossRef]
6. Jithin, K.; Haridev, P.P.; Mayadevi, N.; Harikumar, R.P.; Mini, V.P. A review on challenges in DC microgrid planning and implementation. *J. Mod. Power Syst. Clean Energy* **2023**, *11*, 1375–1395. [CrossRef]
7. Li, Y.; He, J. Distribution system harmonic compensation methods: An overview of DG-interfacing inverters. *IEEE Ind. Electron. Mag.* **2014**, *8*, 18–31. [CrossRef]
8. Kow, K.; Wong, Y.; Kajkumar, R. Power quality analysis for PV grid connected system using PSCAD/EMTDC. *Int. J. Renew. Energy Res.* **2015**, *5*, 121–132.
9. Alhaiz, H.A.; Alsafran, A.S.; Almarhoon, A.H. Single-phase microgrid power quality enhancement strategies: A comprehensive review. *Energies* **2023**, *16*, 5576. [CrossRef]
10. García, Y.; Dufo, R.; Bernal, J. Optimization of isolated hybrid microgrids with renewable energy based on different battery models and technologies. *Energies* **2020**, *13*, 581. [CrossRef]
11. Talluri, G.; Lozito, G.M.; Grasso, F.; García, C.I.; Luchetta, A. Optimal battery energy storage system scheduling within renewable energy communities. *Energies* **2021**, *14*, 8480. [CrossRef]
12. Palizban, O.; Kauhaniemi, K.; Guerrero, J.M. Microgrids in active grid management—Part II: System operation, power quality and protection. *Renew. Sustain. Energy Rev.* **2014**, *36*, 440–451. [CrossRef]
13. Moreira, J.L.; Ferreira, A.; Oliveira, G.; Lima, M.E. Harmonic effects due to the high penetration of photovoltaic generation into a distribution system. *Energies* **2021**, *14*, 4021. [CrossRef]

14. Raghavendra, L.; Parthasarathy, L. Enhancing Power Quality in Microgrids with Integrated Distributed Energy Resources: A Comprehensive Analysis. *J. Propuls. Technol.* **2014**, *55*, 1431–1438.
15. Barbu, V.; Chicco, G.; Corona, F.; Golovanov, N.; Spertino, F. Impact of a Photovoltaic Plant Connected to the MV Network on Harmonic Distortion: An Experimental Assessment. *Sci. Bull.* **2013**, *75*, 179–193.
16. Available online: https://powerquality.blog/2021/07/22/standard-en-50160-voltage-characteristics-of-public-distribution-systems/ (accessed on 3 November 2024).
17. Ostrowska, A.; Michalec, Ł.; Skarupski, M.; Jasiński, M.; Sikorski, T.; Kostyła, P.; Lis, R.; Mudrak, G.; Rodziewicz, T. Power quality assessment in a real microgrid-statistical assessment of different long-term working conditions. *Energies* **2022**, *15*, 8089. [CrossRef]
18. Roy, S.; Debnath, A.; Tariq, M.; Behnamfar, M.; Sarwat, A. Characterizing current THD's dependency on solar irradiance and supraharmonics profiling for a grid–tied photovoltaic power plant. *Sustainability* **2023**, *15*, 1214. [CrossRef]
19. Kaushal, P.; Basak, P. Power quality control based on voltage sag/swell, unbalancing, frequency, THD and power factor using artificial neural network in PV integrated AC microgrid. *Sustain. Energy Grids Netw.* **2020**, *23*, 100365. [CrossRef]
20. Available online: https://standards.ieee.org/ieee/519/10677/ (accessed on 3 November 2024).
21. Jarwar, A.R.; Soomro, A.M.; Memon, Z.A.; Odhano, S.A.; Uqaili, M.A.; Larik, A.S. High dynamic performance power quality conditioner for AC microgrids. *IET Power Electron.* **2019**, *12*, 5264. [CrossRef]
22. Guerrero, N.F.; Batista, R.O.; Ramírez, F.A.; Ferreira, J.; Mercado, R.; Manilla, A. Harmonic Distortion Study of a Photovoltaic Generator in a Microgrid under Disturbances. *Energies* **2024**, *19*, 2031. [CrossRef]
23. Isanbaev, V.; Baños, R.; Martínez, F.; Alcayde, A.; Gil, C. Monitoring Energy and Power Quality of the Loads in a Microgrid Laboratory using Smart Meters. *Energies* **2024**, *17*, 1251. [CrossRef]
24. Liu, Z.; Xu, X.; Abdelsalam, H.A.; Makram, E. Power System Harmonics Study for Unbalanced Microgrid System with PV Sources and Nonlinear Loads. *J. Power Energy Eng.* **2015**, *3*, 43–55. [CrossRef]
25. Andishgar, M.; Gholipour, E. An overview of control approaches of inverter-based microgrids in islanding mode of operation. *Renew. Sustain. Energy Rev.* **2017**, *80*, 1043–1060. [CrossRef]
26. Mohamad, A.; Mohamed, Y. Investigation and assessment of stabilization solutions for DC microgrid with dynamic loads. *IEEE Trans Smart Grid* **2019**, *10*, 5735–5747. [CrossRef]
27. Hernandez, E.; Madrigal-Martínez, M.; Mina-Antonio, J.D.; Iracheta-Cortez, R.; Enríquez-Santiago, J.A.; Rodríguez-Rivera, O.; Martínez-Reyes, G.; Mendoza-Santos, E. A comprehensive review on power quality, optimization techniques, and control strategies of microgrid based on renewable energy sources. *Sustainability* **2023**, *15*, 9847. [CrossRef]
28. Blazek, V.; Petruzela, M.; Vantuch, T.; Slanina, Z.; Misak, S.; Walendziuk, W. The estimation of the influence of household appliances on the power quality in a microgrid system. *Energies* **2020**, *13*, 4323. [CrossRef]
29. Lotfi, H.; Khodaei, A. AC versus DC microgrid planning. *IEEE Trans. Smart Grid* **2017**, *8*, 296–304. [CrossRef]
30. Ma, T.; Cintuglu, M.; Mohammed, O.A. Control of a Hybrid AC/DC microgrid involving energy storage and pulsed loads. *IEEE Trans. Ind. Appl.* **2017**, *53*, 567–575. [CrossRef]
31. *IEEE Std 1547-2018*; IEEE Standard for Interconnection and Interoperability of Distributed Energy Resources with Associated Electric Power Systems Interfaces. IEEE: Piscataway, NJ, USA, 2018; pp. 1–138. [CrossRef]
32. Miridi, S.; Dong, X.; Said, M. Towards hybrid AC/DC micro-grids: Critical analysis and classification of protection strategies. *Renew. Sustain. Energy Rev.* **2018**, *90*, 97–103.
33. Abubakar, M.; Renner, H.; Schurhuber, R. Development of a novel control scheme to achieve the minimum unbalance factor and real power fluctuations under asymmetrical faults. *Energies* **2023**, *16*, 7511. [CrossRef]
34. Macii, D.; Petri, D. Rapid voltage change detection: Limits of the IEC standard approach and possible solutions. *IEEE Trans. Instrum. Meas.* **2020**, *69*, 382–392. [CrossRef]
35. Ghassemi, F.; Perry, M. Review of Voltage Unbalance Limit in the GB Grid Code CC.6.1.5 (b). 2014. Available online: https://www.nationalgrid.com/sites/default/files/documents/37643-Voltage%20Unbalance%20Report.pdf? (accessed on 3 November 2024).
36. *Standard CSA C22.3 No. 9-08-R2015*; Interconnection of Distributed Resources and Electricity Supply Systems. Canadian Standards Association: Toronto, ON, Canada, 2015.
37. Gaur, P.; Singh, S. Investigations on issues in microgrids. *J. Clean Energy Technol.* **2017**, *5*, 47–51. [CrossRef]
38. Li, Y.; Vilathgamuwa, D.; Loh, P. A grid-interfacing power quality compensator for three-phase three-wire microgrid applications. *IEEE Trans. Power Electron.* **2006**, *21*, 1021–1031. [CrossRef]
39. Khan, M.; Haque, A.; Kurukuru, V.; Wang, H.; Blaabjerg, F. Standalone operation of distributed generation systems with improved harmonic elimination scheme. *IEEE J. Emerg. Sel. Top. Power Electron.* **2021**, *9*, 6924–6934. [CrossRef]
40. Martínez, M.; Burgos-Mellado, C.; Morales-Paredes, H.K.; Gómez, J.S.; Verma, A.K.; Bonaldo, J.P. Distributed control scheme for clusters of power quality compensators in grid-tied AC microgrids. *Sustainability* **2023**, *15*, 15698. [CrossRef]
41. Blooming, T.; Carnovale, D. Application of IEEE Std. 519-1992 harmonic limits. In Proceedings of the Conference Record of 2006 Annual Pulp and Paper Industry Technical Conference, Appleton, WI, USA, 18–23 June 2006.
42. Cho, N.; Lee, H.; Bhat, R.; Heo, K. Analysis of harmonic hosting capacity of IEEE Std. 519 with IEC 61000-3-6 in distribution systems. In Proceedings of the 2019 IEEE PES GTD Grand International Conference and Exposition Asia (GTD Asia), Bangkok, Thailand, 19–23 March 2019.

43. Gao, D.W.; Muljadi, E.; Tian, T.; Miller, M.; Wang, W. *Comparison of Standards and Technical Requirements of Grid-Connected Wind Power Plants in China and the United States*; Technic Report NREL/TP-5D00-64225; National Renewable Energy Lab.: Golden, CO, USA, 2016.
44. Nejabatkhah, F.; Li, Y. Overview of power management strategies of hybrid AC/DC microgrid. *IEEE Trans. Power Electron.* **2015**, *30*, 7072–7089. [CrossRef]
45. Mayoral, E.H.; Reyes, E.D.; Cortez, R.I.; Hernández, C.J.; Gómez, C.D.; Román, C.R.; Romero, J.D.; Rivera, O.R.; Santos, E.F.; Gómez, W.D.; et al. *Power Quality in Renewable Energy Microgrids Applications with Energy Storage Technologies: Issues, Challenges and Mitigations*; IntechOpen: London, UK, 2022.
46. Micallef, A.; Apap, M.; Spiteri, C.; Guerrero, J.M. Mitigation of harmonic in grid-connected and islanded micro-grids via virtual admittances and impedances. *IEEE Trans. Smart Grid* **2017**, *8*, 651–661.
47. Tran, T.S.; Nguyen, D.T.; Fujita, G. The analysis of technical trend in islanding operation, harmonic distortion, stabilizing frequency, and voltage of islanded entities. *Resources* **2019**, *8*, 14. [CrossRef]
48. Shafiefi, A.; Dehkordi, M.; Kiyoumarsi, A.; Farhangi, S. A Control Approach for Small–Scale PMSG–based WECS in the Whole Wind Speed Range. *IEEE Trans. Power Electron.* **2017**, *23*, 9117–9130. [CrossRef]
49. Cao, J.; Emadi, A.A. New Battery/UltraCapacitor Hybrid Energy Storage System for Electric, Hybrid, and Plug-In Hybrid Electric Vehicles. *IEEE Trans. Power Electron.* **2012**, *27*, 122–132.
50. Khaligh, A.; Li, Z. Battery, Ultracapacitor, Fuel Cell, and Hybrid Energy Storage Systems for Electric, Hybrid Electric, Fuel Cell, and Plug-In Hybrid Electric Vehicles: State of the Art. *IEEE Trans. Veh. Technol.* **2010**, *59*, 2806–2814. [CrossRef]
51. Martha, S.K.; Elias, L. Nanostructured Anode Materials for Batteries (Lithium Ion, Ni-MH, Lead-Acid, and Thermal Batteries). In *Nanomaterials for Electrochemical Energy Storage Devices*; John Wiley & Sons, Ltd.: Hoboken, NJ, USA, 2019; Chapter 3; pp. 145–229.
52. Bizuayehu, A.W.; Medina, P.; Catalão, J.P.S.; Rodrigues, E.M.G.; Contreras, J. Analysis of Electrical Energy Storage Technologies state-of-the-Art and Applications on Islanded Grid Systems. In Proceedings of the 2014 IEEE PES T D Conference and Exposition, Chicago, IL, USA, 14–17 April 2014; pp. 1–5.
53. Zhang, H.; Sun, C. Cost-effective iron-based aqueous redox flow batteries for large-scale energy storage application: A review. *J. Power Sources* **2021**, *493*, 229445. [CrossRef]
54. Faisal, M.; Hannan, M.A.; Ker, P.J.; Hussain, A.; Mansor, M.B.; Blaabjerg, F. Review of energy storage system technologies in microgrid applications: Issues and challenges. *IEEE Access* **2018**, *6*, 35143–35164. [CrossRef]
55. Georgious, R.; Refaat, R.; Garcia, J.; Daoud, A.A. Review on energy storage systems in microgrids. *Electronics* **2021**, *10*, 2134. [CrossRef]
56. Shabestary, M.M.; Mohamed, Y.A.R.I. Autonomous coordinated control scheme for cooperative asymmetric low-voltage ride-through and grid support in active distribution networks with multiple DG units. *IEEE Trans. Smart Grid* **2020**, *11*, 2125–2139. [CrossRef]
57. Arranz, A.; Zorita, A.; Morinigo, D.; Duque, O. A review of total harmonic distortion factors for the measurement of harmonic and inter-harmonic pollution in modern power systems. *Energies* **2021**, *14*, 6467. [CrossRef]
58. Wu, Y.; Lin, J.; Lin, H. Standards and guidelines for grid–connected photovoltaic generation systems: A review and comparison. *IEEE Trans. Ind. Appl.* **2017**, *53*, 3205–3216. [CrossRef]
59. Padayattil, G.M.; Thobias, T.; Thomas, M.; Sebastian, J.; Pathirikkat, G. Harmonic analysis of microgrid operation in islanded mode with non–linear loads. In Proceedings of the 2016 International Conference on Computer Communication and Informatics (ICCCI), Coimbatore, India, 7–9 January 2016.
60. Available online: https://cdn.standards.iteh.ai/samples/19103/f419cf3a1a1e4a179aae2276e6514bb7/IEC-60831-2-2014.pdf (accessed on 3 November 2024).